Journal of Scientific Computing (2026) 107:68
https://doi.org/10.1007/s10915-026-03286-9

Projective Integration Schemes for Nonlinear Degenerate Parabolic Systems

Tommaso Tenna[1,2]

Received: 6 March 2025 / Revised: 19 February 2026 / Accepted: 24 March 2026 /
Published online: 9 April 2026

Abstract
A general high-order fully explicit scheme based on projective integration methods is here presented to solve systems of degenerate parabolic equations in general dimensions. The method is based on a BGK approximation of the advection-diffusion equation, where we introduce projective integration method as time integrator to deal with the stiff relaxation term. This approach exploits the clear gap in the eigenvalues spectrum of the kinetic equation, taking into account a sequence of small time steps to damp out the stiff components, followed by an extrapolation step over a large time interval. The time step restriction on the projective step is similar to the CFL condition for advection-diffusion equations. In this paper we discuss the stability and the consistency of the method, presenting some numerical simulations in one and two spatial dimensions.

Keywords Advection-diffusion equations · Relaxation schemes · High-order methods · Projective integration

Mathematics Subject Classification 65M08 · 65L04 · 65M12

1 Introduction

The numerical study of degenerate parabolic equations has gained particular interest in the last decades. These problems arise in several physical applications, such as flow of gas in porous media [18], radiative transport [49] or cell chemotactic movement [47]. The numerical approximation of these equations is challenging due to the presence of possible degenerate points, in which the parabolic system loses its properties, exhibiting hyperbolic behavior with finite speed of propagation and sharp fronts. In general, classical solutions might not exist even for C^2 initial data and weak solutions must be considered. Many different schemes have been proposed to solve degenerate parabolic equations, such as local discontinuous Galerkin methods [54], mixed finite element methods [3], central finite volume schemes [31], finite

✉ Tommaso Tenna
tommaso.tenna@univ-cotedazur.fr; tommaso.tenna@uniroma1.it

1 Université Côte d'Azur, CNRS, LJAD, Parc Valrose, F-06108 Nice, France

2 Dipartimento di Matematica Guido Castelnuovo, Sapienza Università di Roma, P.le Aldo Moro 5, 00185 Roma, Italy

volume schemes preserving steady-states [10], high order finite difference WENO schemes [39], residual distribution schemes [1] and WENO schemes based on deep learning techniques [30]. Among these methods, a discrete kinetic approximation of these equations have been proposed by Aregba-Driollet, Natalini and Tang [7], inspired by relaxation schemes [6, 25] and kinetic approximation of hydrodynamic equations in the hyperbolic setting [37]. The idea relies on a Bhatnagar-Gross-Krook (BGK) approximation of the macroscopic equation, where both the kinetic velocities and the source term depend singularly on the relaxation parameter. Different relaxation systems for the approximation of degenerate parabolic equations have been proposed in [42, 44], with high-order extension developed in [16], where the authors coupled ENO and WENO schemes for space discretization with IMEX schemes for time advancement. This approach is inspired by kinetic schemes for the Carleman model, but the numerical integration is directly performed at the macroscopic level. In the context of relaxation schemes, other diffusive kinetic models and approximations have been proposed, see for instance [24, 38, 43].

The main advantage of relaxation schemes is the possibility to treat the scalar and the system case in the same way at the numerical level, with the feasibility of parallelizing the algorithm due to the diagonal form of the approximating problems. Indeed discrete kinetic approximations are based on linear hyperbolic terms, whose structure is very likely for numerical and theoretical purpose [6, 7, 45]. The nonlinearity inside the derivatives is replaced by a semilinearity: the differential part becomes linear and all the nonlinearity is concentrated inside the source term. On the other hand, the main disadvantage of this approach is the appearance of a stiff source term, describing the relaxation of the new variable towards the equilibrium, which requires suitable time integrators.

In this perspective, the idea is to use an efficient explicit time integrator which is able to speed up the computation due to the particular structure of the kinetic formulation. Several systems are characterized by the coexistence of processes evolving on widely different time scales, where certain dynamics are much faster than others. These distinct dynamical behaviors correspond to eigenvalues of different magnitudes: the fast modes (associated with eigenvalues having large negative part) decay rapidly, whereas the slow modes are the active components, still present in the solution. Systems exhibiting such a strong disparity of time scales are referred to as *stiff*. This scale separation appears as a gap in the spectrum of the system operator, requiring specific numerical methods. Indeed, the presence of fast, strongly damped components imposes severe restrictions on explicit time-stepping methods.

In the context of kinetic equations, two main mechanisms act on different time scales: collisions, which are typically fast and quickly damp out microscopic fluctuations, and advection, which is slow and governs macroscopic transport over much longer time scales.

Projective integration method was introduced in [20] as a technique to accelerate a brute-force integration of stiff systems of ordinary differential equations, which require restrictive conditions on the time step. The idea, extended in [34] for kinetic equations with a diffusive scaling, is based on an extrapolation in time over a large time step, performed after taking a few inner steps to damp out the transient corresponding to the fast modes. Several extensions have been proposed both for hyperbolic problems [33] and for high order approximation of kinetic equations [32]. We mention also telescopic projective integration techniques, where the projective integration method have been extended to deal with problems having multiple time scales, both for ODEs systems [21] and for kinetic equations [8, 40, 41]. Applications of projective integration techniques to hyperbolic moment models have been recently investigated in [2, 27, 28], obtaining accurate, but efficient simulations with significant speed up.

In [7, 16] the methods are based on splitting techniques, restricting the order in time to 2. The order of convergence in time could be increased by solving explicitly the BGK equation, without projecting over the Maxwellian space. Many asymptotic-preserving schemes based on IMEX techniques have been proposed to integrate stiff kinetic equations and we refer to the recent survey [11] for a detailed analysis on the topic.

Aim of the Paper

The goal of this paper is to propose a fully explicit and robust projective integration scheme to numerically solve the stiff BGK system with arbitrary order of accuracy in time, extending the idea of [33] to the case of possibly degenerate parabolic systems. The main contribution of the manuscript is given by the analysis of the spectrum for the discrete-BGK approximation, along with the identification of the parameters for the projective integration scheme. This analysis justifies the speed up of the method compared to classical time integrators.

Structure of the Paper

The plan of the paper is the following: in Section 2 we introduce discrete kinetic relaxation schemes for convection-diffusion equations, investigating different models. We construct the numerical scheme, focusing on the phase space discretization. In Section 3 we introduce projective integration method to treat the time discretization with a fully explicit approach, by exploiting the particular structure of the BGK operator. Based on [32], we investigate the spectrum of the operator and we perform stability and consistency analysis of the method. In Section 4 we present some numerical simulations in both one and two space dimensions for different problems. All the details about the numerical schemes are reported in the Appendix.

2 Relaxation Schemes for Nonlinear Degenerate Parabolic Systems

In this section, we study discrete kinetic schemes for systems of conservation laws with possibly degenerate diffusion, referring to [7], but other kinetic models and approximations can be built, see for instance [24]. Let $u : \mathbb{R}^D \times \mathbb{R}^+ \to \mathbb{R}^K$, $D > 0$, $K > 0$, be a weak solution of the following system

$$\partial_t u + \sum_{d=1}^{D} \partial_{x_d} A_d(u) = \Delta_x B(u), \qquad (x, t) \in \mathbb{R}^D \times (0, +\infty), \tag{1}$$

for a given initial condition

$$u(x, 0) = u_0(x), \qquad x \in \mathbb{R}^D. \tag{2}$$

Here t defines the time, x_d defines the spatial variable for each dimension $d = 1, \dots, D$ and $u_0 : \mathbb{R}^D \to \mathbb{R}^K$. The functions $A_d : \mathbb{R}^K \to \mathbb{R}^K$ and $B : \mathbb{R}^K \to \mathbb{R}^K$ are assumed to be Lipschitz-continuous. In addition, for all u lying in a fixed domain $\Omega \in \mathbb{R}^D$ it holds true:

- For all $\xi \in \mathbb{R}^D$, $\sum_{d=1}^{D} \xi_d A_d'(u)$ has real eigenvalues and it is diagonalizable,
- $B'(u)$ has real non- negative eigenvalues.

Here, A' and B' denote the differentials of A and B, respectively. This notation will be used throughout the whole paper.
In [6] a family of discrete diffusive kinetic schemes has been proposed, in order to construct a numerical approximation of the original system (1). Let us consider $f^\varepsilon = (f_1^\varepsilon, \dots f_L^\varepsilon)$ as the solution of the following kinetic model in general form:

$$\begin{cases} \partial_t f^\varepsilon + \sum_{d=1}^{D} \Gamma_d^\varepsilon \, \partial_{x_d} f^\varepsilon = \frac{1}{\varepsilon}(\mathcal{M}(\varepsilon, u^\varepsilon) - f^\varepsilon), \\ u^\varepsilon(x,t) = \sum_{l=1}^{L} f_l^\varepsilon(x,t), \end{cases} \tag{3}$$

where $f_l^\varepsilon : \mathbb{R}^D \times \mathbb{R}^+ \to \mathbb{R}^K$, $L > 0$ is the number of discrete velocites and let us take the initial condition

$$f^\varepsilon(x,0) = f_0^\varepsilon(x). \tag{4}$$

Here $\mathcal{M}_l : \mathbb{R}^+ \times \mathbb{R}^K \to \mathbb{R}^K$ are the Maxwellian functions for each $l = 1, \dots, L$ and $\Gamma_d^\varepsilon \in \mathbb{R}^{LK \times LK}$ are constant diagonal matrices, consisting in L diagonal blocks of size $K \times K$L diagonal blocks of size, each equal to a scalar multiple of the identity matrix, where the diagonal entries γ_{ld}^ε are given by

$$\gamma_{ld}^\varepsilon := \lambda_{ld} + \frac{\theta_{ld}}{\sqrt{\varepsilon}}, \tag{5}$$

for some fixed real constants λ_{ld}, θ_{ld}. The relaxation parameter $\varepsilon > 0$ can be a physical parameter or an artificial one and the kinetic system (3) converges (at least formally) to the original macroscopic system (1) as $\varepsilon \to 0$, under an analogous of the *subcharacteristic condition* [46] (which ensures that the relaxation waves propagate no faster than the equilibrium waves, guaranteeing consistency with the original system).

The Maxwellian $\mathcal{M}$ essentially embeds the macroscopic variable u^ε in the kinetic space and the right hand side models a relaxation of the kinetic variable f^ε towards the equilibrium state given by the Maxwellian $\mathcal{M}$. From now on, let us consider $\Omega \in \mathbb{R}^K$ a convex and compact domain (see [12]), such that $u(x,t) \subset \Omega$ for all $(x,t) \in \mathbb{R}^D \times \mathbb{R}^+$. In Section 2.1 we show that, in the limit $\varepsilon \to 0$, the kinetic approximation formally converges to the macroscopic model under some fundamental assumptions on the Maxwellian functions:

(M1) $\sum_{l=1}^{L} \mathcal{M}_l(\varepsilon, w) = w$ for all $\varepsilon \in (0,1]$ and for all $w \in \Omega$,

(M2) $\sum_{l=1}^{L} \gamma_{ld}^\varepsilon \, \mathcal{M}_l(\varepsilon, w) = A_d(w)$ for all $\varepsilon \in (0,1]$ and for all $w \in \Omega$, for all $d = 1, \dots, D$,

(M3) $\sum_{l=1}^{L} \theta_{ld}\theta_{lj} \mathcal{M}_l(0, w) = \delta_{dj} B(w)$ for all $w \in \Omega$, for all $d, j = 1, \dots, D$,
where $\delta_{\cdot,\cdot}$ is the Kronecker symbol,

(M4) $\mathcal{M}_l(\varepsilon, w) \to \mathcal{M}_l(0, w)$ when $\varepsilon \to 0$ uniformly for $w \in \Omega$, *i.e.* $\forall \nu > 0$, there exists $\delta > 0$ uniform in w and depending only on Ω such that for all $\varepsilon < \delta$ and $w \in \Omega$

$$|\mathcal{M}_l(\varepsilon, w) - \mathcal{M}_l(0, w)| \le \nu,$$

in a suitable norm [7].

Definition 1 A Lipschitz continuous function $\mathcal{M}$ is a (local) Maxwellian Function for system (1) with respect to the interval Ω if (M1)-(M4) are satisfied.

If $\mathcal{M}$ satisfies the above conditions it is called a local Maxwellian Function for system (1) on Ω. Let us recall that in discrete-BGK models, the projection onto macroscopic quantities is equivalent to the classical averaging procedure used in continuous kinetic theory [17]; however, since the velocity space is discrete, the integral becomes a finite summation over the discrete velocities. Hence, the first property tells us that the projection of the Maxwellian is the identity, which means that considering a given macroscopic variable embedded in the microscopic space and projecting it back, we obtain the original state. The second property and the third property are necessary to guarantee the consistency with the macroscopic fluxes and, therefore, to preserve the structure of the macroscopic model in the limit of the kinetic model (3) towards (1). The last property is fundamental to obtain a uniform convergence with respect to ε, when $\varepsilon \to 0$.

The stability condition for this model deals with the following definition.

Definition 2 A local Maxwellian function is a monotone Maxwellian function (MMF) if for all $l \in \{1, \dots, L\}$, for all positive $\varepsilon \leq 1$ and for all $u \in \Omega$, the real parts of the eigenvalues of $\mathcal{M}_l'(\varepsilon, u)$ are non-negative.

Henceforth, the explicit dependence of the Maxwellian on ε will be omitted whenever unnecessary.

Rigorous theoretical results about the convergence of the solution to the BGK model (3) towards a weak solution to the system (1) have been proven for the scalar case in [13] and for a class of one dimensional strongly degenerate parabolic systems in [35].

In the next subsection we give a formal derivation of the macroscopic equation, starting from the Chapman-Enskog expansion and assuming the properties (M1)-(M4).

2.1 Chapman-Enskog Expansion

Let us define the matrix $P \in \mathbb{R}^{K \times LK}$, where the map $f^\varepsilon \mapsto Pf^\varepsilon$ is a projection onto the Maxwellian manifold, and the auxiliary variables

$$u^\varepsilon := P\, f^\varepsilon = \sum_{l=1}^{L} f_l^\varepsilon, \qquad v_d^\varepsilon = P\, \Gamma_d\, f^\varepsilon = \sum_{l=1}^{L} \gamma_{ld}^\varepsilon\, f_l^\varepsilon \qquad d = 1, \dots, D. \tag{6}$$

Then from (3) and the compatibility assumptions (M1)-(M4), we have

$$\begin{cases} \partial_t u^\varepsilon + \displaystyle\sum_{d=1}^{D} \partial_{x_d} v_d^\varepsilon = 0, \\ \partial_t v_d^\varepsilon + \displaystyle\sum_{j=1}^{D} \partial_{x_j} \left(P\, \Gamma_d \Gamma_j\, f^\varepsilon \right) = \dfrac{1}{\varepsilon} \left(A_d(u^\varepsilon) - v_d^\varepsilon \right). \end{cases} \tag{7}$$

Let us consider a formal Chapman-Enskog expansion of f^ε in the form

$$f^\varepsilon = \mathcal{M}(u^\varepsilon) + \sqrt{\varepsilon}\, g^\varepsilon + \mathcal{O}(\varepsilon). \tag{8}$$

Then, by multiplying $(7)_2$ by ε and using the explicit expression of P, one has

$$v_d^\varepsilon = A_d(u^\varepsilon) - \varepsilon \left(\partial_t v_d^\varepsilon + \sum_{j=1}^{D} \partial_{x_j} \sum_{l=1}^{L} \gamma_{dj} \gamma_{lj}\, f_l^\varepsilon \right). \tag{9}$$

Expanding the expression of γ_{lj}, this can be rewritten as

$$\begin{aligned} v_d^\varepsilon &= A_d(u^\varepsilon) - \sum_{l=1}^{L}\sum_{j=1}^{D} \theta_{ld}\theta_{lj}\partial_{x_j} f_l^\varepsilon + \mathcal{O}(\sqrt{\varepsilon}) \\ &= A_d(u^\varepsilon) - \sum_{l=1}^{L}\sum_{j=1}^{D} \theta_{ld}\theta_{lj}\partial_{x_j} \mathcal{M}_l(u^\varepsilon) + \mathcal{O}(\sqrt{\varepsilon}). \end{aligned} \tag{10}$$

Using (M3) and (M4), this implies that

$$\partial_t u^\varepsilon + \sum_{d=1}^{D} \partial_{x_d} A_d(u^\varepsilon) = \Delta_x B(u^\varepsilon) + \mathcal{O}(\sqrt{\varepsilon}). \tag{11}$$

This formal justification shows that the natural convergence rate in (M4) would be $\sqrt{\varepsilon}$. The rigorous proof of this result has been obtained in [13], using a priori bounds on the discrete velocity BGK approximation and kinetic entropy inequalities.

2.2 Discrete Kinetic Models

In the pure hyperbolic setting, system (3) reduces to the one developed in [45] and [6]. Let us consider the following hyperbolic system of conservation laws

$$\partial_t u + \sum_{d=1}^{D} \partial_{x_d} A_d(u) = 0, \tag{12}$$

and the following approximating discrete BGK model

$$\begin{cases} \partial_t f_l^\varepsilon + \displaystyle\sum_{d=1}^{D} \lambda_{ld}\partial_{x_d} f_l^\varepsilon = \frac{1}{\varepsilon}(\tilde{\mathcal{M}}_l(u^\varepsilon) - f_l^\varepsilon), \qquad l = 1, \dots, J, \\ u^\varepsilon = P\, f^\varepsilon = \displaystyle\sum_{l=1}^{J} f_l^\varepsilon, \end{cases} \tag{13}$$

where $\tilde{\mathcal{M}}_l$ are Maxwellian functions and J is the number of velocities needed to approximate the hyperbolic equation, complemented with the compatibility conditions

$$\sum_{l=1}^{J} \tilde{\mathcal{M}}_l(u) = u, \qquad \sum_{l=1}^{J} \lambda_{ld}\tilde{\mathcal{M}}_l(u) = A_d(u), \qquad \forall u \in \Omega, \quad d = 1, \dots, D. \tag{14}$$

In [45] it has been shown that the solution of the discrete BGK model (13), under the hypothesis of monotone Maxwellian functions, converges to the unique entropy solution of the hyperbolic system (12), see also [46].

In the same spirit, a model for (1) can be obtained by adding linear combinations of B to the $\tilde{\mathcal{M}}_l$, together with supplementary equations to take into account the diffusive scaling. More precisely, fixing $J' \geq D+1$ the number of velocities you need to deal with the parabolic

term and $L = J + J'$, we can design the model as

$$\begin{cases} \partial_t f_l^\varepsilon + \sum_{d=1}^{D} \lambda_{ld}^\varepsilon \partial_{x_d} f_l^\varepsilon = \frac{1}{\varepsilon}(\tilde{\mathcal{M}}_l(u^\varepsilon) - f_l^\varepsilon), \qquad 1 \le l \le J, \\ \partial_t f_{J+m}^\varepsilon + \left(\mu + \frac{\theta\sqrt{J'}}{\sqrt{\varepsilon}}\right) \sum_{d=1}^{D} \sigma_{md}^\varepsilon \partial_{x_d} f_{J+m}^\varepsilon = \frac{1}{\varepsilon}\left(\frac{B(u^\varepsilon)}{J'\theta^2} - f_{J+m}^\varepsilon\right), \qquad 1 \le m \le J', \\ u^\varepsilon(x,t) = \sum_{l=1}^{L} f_l^\varepsilon(x,t). \end{cases} \tag{15}$$

In a compact form, the kinetic model reads as

$$\partial_t f^\varepsilon + \Gamma^\varepsilon \partial_x f^\varepsilon = \frac{1}{\varepsilon}(\mathcal{M}(u^\varepsilon) - f^\varepsilon). \tag{16}$$

In particular, for $1 \le l \le J$:

$$\mathcal{M}_l(u) = \tilde{\mathcal{M}}_l(u) + b_l B(u), \tag{17}$$

where $b_l \in \mathbb{R}$. On the other hand, for the last J' equations, we have

$$\theta_l = \theta \ge 0, \ \lambda_l = \mu \ge 0, \qquad \text{for} \quad l = 1, \dots, J' \tag{18}$$

and $\{\sigma_d^\varepsilon\}_{d=1}^D$ are orthonormal vectors in $\{X \in \mathbb{R}^{J'} \text{ s.t. } \sum_{m=1}^{J'} X_m = 0\} =: \mathcal{H}$. From a numerical point of view, the orthonormality automatically implies that the multi-dimensional problem can be treated independently along each direction.

For the sake of completeness, we provide some concrete and specific examples of this strategy, describing three models which can be applied in one and two space dimensions. We will observe in the following subsections that all these proposed models satisfy the monotonicity condition, as already observed in [7].

2.2.1 Diagonal Relaxation Model 1 (DRM1)

Let us first focus on the one-dimensional case, where we choose $J = 2$ and $J' = 2$. The kinetic model reads as in (16), where

$$\begin{cases} \Gamma^\varepsilon = \text{diag}\left(\lambda_1, \lambda_2, -\frac{\mu}{\sqrt{2}} - \frac{\theta}{\sqrt{\varepsilon}}, \frac{\mu}{\sqrt{2}} + \frac{\theta}{\sqrt{\varepsilon}}\right)^T, \\ \mathcal{M}(u) = \frac{1}{2}\left(u + \frac{A(u)}{\lambda_1} - \frac{B(u)}{\theta^2}, u + \frac{A(u)}{\lambda_2} - \frac{B(u)}{\theta^2}, \frac{B(u)}{\theta^2}, \frac{B(u)}{\theta^2}\right)^T, \end{cases} \tag{19}$$

where $\lambda_1, \lambda_2, \theta, \mu \in \mathbb{R}$. For the sake of notation, we set $\lambda_2 = -\lambda_1 = \lambda > 0$. Note that the Maxwellian functions do not depend anymore on ε.

Let us suppose that for all u, $A'(u)$ and $B'(u)$ have a basis of common eigenvectors, denoting $\lambda_k(U)$ and $\theta_k^2(u)$ their respective eigenvalues for $1 \le k \le K$ (K is the number of components of u in (1)) and let us assume that the eigenvalues of B' are real, then $\mathcal{M}$ is a Monotone Maxwellian Function if

$$\sup_{u \in \Omega} \sup_{1 \le k \le K} \frac{|\lambda_k(u)|}{\lambda} + \frac{\theta_k^2(u)}{\theta^2} \le 1, \tag{20}$$

which is a generalized subcharacteristic condition [7], retrieving the hyperbolic one [6, Proposition 3.2] for $\theta = 0$.

Let us consider now the two-dimensional model, in which $J' \geq D + 1 = 3$, $\theta > 0$, $\mu \geq 0$. Let $\{\sigma^{(1)}, \sigma^{(2)}\}$ be orthonormal in $\mathcal{H}$, then we consider the following velocities $\gamma_{ld}^{\varepsilon}$, introduced in (5) for the general setting

$$\gamma_1^{\varepsilon} = \begin{pmatrix} \lambda_1(-1,0,1)^T \\ \left(\mu + \dfrac{\theta\sqrt{J'}}{\sqrt{\varepsilon}}\right)\sigma^{(1)} \end{pmatrix}, \quad \gamma_2^{\varepsilon} = \begin{pmatrix} \lambda_2(0,-1,1)^T \\ \left(\mu + \dfrac{\theta\sqrt{J'}}{\sqrt{\varepsilon}}\right)\sigma^{(2)} \end{pmatrix}, \tag{21}$$

where $\lambda_2 = -\lambda_1 = \lambda > 0$. Let us consider the following Maxwellian functions:

$$\mathcal{M}(u) = \frac{1}{3}\begin{pmatrix} u - 2\dfrac{A_1(u)}{\lambda_1} + \dfrac{A_2(u)}{\lambda_2} \\ u + \dfrac{A_1(u)}{\lambda_1} - 2\dfrac{A_2(u)}{\lambda_2} \\ u + \dfrac{A_1(u)}{\lambda_1} + \dfrac{A_2(u)}{\lambda_2} \\ (0,\dots,0)^T \end{pmatrix} + \frac{B(u)}{\theta^2}\begin{pmatrix} -\dfrac{1}{3}(1,1,1)^T \\ \dfrac{1}{J'}(1,\dots,1)^T \end{pmatrix}. \tag{22}$$

In the scalar case ($K = 1$), the Maxwellian $\mathcal{M}\colon \mathbb{R} \to \mathbb{R}^{3+J'}$ is a MMF if the following condition is satisfied:

$$\max_{u\in I}\left(\frac{2\,A_1'}{\lambda_1} - \frac{A_2'}{\lambda_2}, -\frac{A_1'}{\lambda_1} + \frac{2\,A_2'}{\lambda_2}, -\frac{A_1'}{\lambda_1} - \frac{A_2'}{\lambda_2}\right) \leq 1 - \frac{B'}{\theta^2}, \tag{23}$$

which is equivalent to the subcharacteristic condition presented in [6, Proposition 3.2], for the hyperbolic case $\theta = 0$ and $B \equiv 0$.

2.2.2 Diagonal Relaxation Model 2 (DRM2)

In this model, we consider the same structure as (DRM1) replacing $-\lambda$ by λ_m and λ by λ_p. In the one-dimensional case the kinetic model is given by (16), where now

$$\begin{cases} \Gamma^{\varepsilon} = \operatorname{diag}\left(\lambda_m, \lambda_p, -\dfrac{\mu}{\sqrt{2}} - \dfrac{\theta}{\sqrt{\varepsilon}}, \dfrac{\mu}{\sqrt{2}} + \dfrac{\theta}{\sqrt{\varepsilon}}\right)^T, \\ \mathcal{M}_1(u) = \dfrac{1}{\lambda_p - \lambda_m}\left(\lambda_p\left(u - \dfrac{B(u)}{\theta^2}\right) - A(u)\right), \\ \mathcal{M}_2(u) = \dfrac{1}{\lambda_p - \lambda_m}\left(-\lambda_m\left(u - \dfrac{B(u)}{\theta^2}\right) + A(u)\right), \\ \mathcal{M}_3(u) = \mathcal{M}_4(u) = \dfrac{B(u)}{2\,\theta^2}. \end{cases} \tag{24}$$

Supposing without loss of generality that $\lambda_m < \lambda_p$, the Maxwellian $\mathcal{M}$ is a MMF if

$$\lambda_m\left(1 - \frac{B'(u)}{\theta^2}\right) \leq A'(u) \leq \lambda_p\left(1 - \frac{B'(u)}{\theta^2}\right), \qquad \forall\, u \in \Omega, \tag{25}$$

which is readily satisfied under the hypothesis

$$1 - \frac{B'(u)}{\theta^2} > 0 \qquad \forall\, u \in \Omega. \tag{26}$$

This condition allows for a sharper approximation of A' than (23), suggesting that the numerical approximation could provide better results [7]. More specifically, we take

$$\lambda_m = \inf_{u\in\Omega} \frac{A'(u)}{1 - B'(u)/\theta^2}, \qquad \lambda_p = \sup_{u\in\Omega} \frac{A'(u)}{1 - B'(u)/\theta^2}, \tag{27}$$

to guarantee the maximality of λ_m and the minimality of λ_p.

2.2.3 A 3 Velocities Model (OVM)

For the sake of completeness, we show another choice for the kinetic model, characterized by orthogonal velocities and ε-dependent Maxwellians in (16) where

$$\begin{cases} \Gamma^\varepsilon = \mathrm{diag}\,(0, \lambda, -\lambda)\,, \\ \mathcal{M}_1(\varepsilon, u) = u - \dfrac{B(u)}{\theta^2}, \\ \mathcal{M}_2(\varepsilon, u) = \dfrac{\left(\lambda + \frac{\theta}{\sqrt{\varepsilon}}\right)}{2\left|\lambda + \frac{\theta}{\sqrt{\varepsilon}}\right|^2} A(u) + \dfrac{B(u)}{2\theta^2}, \\ \mathcal{M}_3(\varepsilon, u) = -\dfrac{\left(\lambda + \frac{\theta}{\sqrt{\varepsilon}}\right)}{2\left|\lambda + \frac{\theta}{\sqrt{\varepsilon}}\right|^2} A(u) + \dfrac{B(u)}{2\theta^2}. \end{cases} \tag{28}$$

In this case, if the equation (1) does not degenerate or for instance

$$B'(u) \geq |A'(u)| \tag{29}$$

holds, then the monotonicity conditions are verified for ε small if $\theta^2 > \max B'$. Indeed, by computing derivatives of Maxwellian functions, we obtain

$$\begin{cases} \mathcal{M}_1'(u) &= 1 - \dfrac{B'(u)}{\theta^2}, \\ \mathcal{M}_2'(u) &= C(\varepsilon)\, A'(u) + \dfrac{B'(u)}{2\theta^2}, \\ \mathcal{M}_3'(u) &= -\,C(\varepsilon)\, A'(u) + \dfrac{B'(u)}{2\theta^2}, \end{cases} \tag{30}$$

where

$$C(\varepsilon) = \frac{\lambda + \frac{\theta}{\sqrt{\varepsilon}}}{2\left|\lambda + \frac{\theta}{\sqrt{\varepsilon}}\right|^2}. \tag{31}$$

This implies that $B'(u) \leq \theta^2$ and

$$\frac{B'(u)}{\theta^2} \geq 2\big|C(\varepsilon)\big|\,|A'(u)|. \tag{32}$$

When the macroscopic equation (1) is degenerate, i.e. $B'(u) = 0$ for some $u \in \Omega$, then Equation (32) cannot be satisfied. Conversely, if $B'(u) \geq |A'(u)|$ and $B'(u) \leq \theta^2$, the monotonicity conditions are ensured for sufficiently small ε.

Remark 1 It is important to observe that by approximating the original system (1) with a kinetic model of the form (3), a modeling error is introduced and it is strictly ε-dependent, as can be seen from the Chapman-Enskog expansion in Section 2.1. However, in any numerical

approximation of this model, a nonzero value of ε must be taken. This choice is dictated by the consistency of the numerical schemes with respect to the original problem.

2.3 Numerical Approximation

The main goal is to avoid splitting techniques to numerically solve (15) to obtain high order approximation. Indeed, simple splitting techniques are inherently first order, while achieving high order is much more complicated and introduces stability issues.
First, we introduce a phase space discretization using a discrete velocity model among the ones introduced above, coupled with a finite volume scheme for the advection term. This leads to a semidiscrete version of the system (3) of the form:

$$\frac{d f}{dt} = D_t^{\varepsilon}(f). \tag{33}$$

In our setting, D_t^{ε} is the semidiscrete operator given by

$$D_t^{\varepsilon}(f) = -\Phi^{\varepsilon}(f) + \frac{1}{\varepsilon}\left(\mathcal{M}(u) - f\right), \tag{34}$$

where Φ^{ε} is a suitable discretization of the convective derivative, as discussed in the remainder of this section. This equation is characterized by the presence of two different time scales (one governing the advection and the other governing collisions). To this aim, we propose a projective integration scheme for the time discretization.

2.3.1 Velocity Discretization

Let us rewrite explicitly the semidiscrete problem (33) in the two dimensional version:

$$\begin{cases} \partial_t f_l^{\varepsilon} + \lambda_{l1}\partial_x f_l^{\varepsilon} + \lambda_{l2}\partial_y f_l^{\varepsilon} = \dfrac{1}{\varepsilon}\left(\mathcal{M}_l(u^{\varepsilon}) - f_l^{\varepsilon}\right), & 1 \le l \le J, \\ \partial_t f_{J+m}^{\varepsilon} + \left(\dfrac{\mu}{\sqrt{2}} + \dfrac{\theta}{\sqrt{\varepsilon}}\right)\sigma_{J+m}^{(1)}\partial_x f_{J+m}^{\varepsilon} \\ \qquad + \left(\dfrac{\mu}{\sqrt{2}} + \dfrac{\theta}{\sqrt{\varepsilon}}\right)\sigma_{J+m}^{(2)}\partial_y f_{J+m}^{\varepsilon} = \dfrac{1}{\varepsilon}\left(\dfrac{B(u^{\varepsilon})}{2\theta^2} - f_{J+m}^{\varepsilon}\right), & 1 \le m \le J' \\ u^{\varepsilon}(x,t) = \displaystyle\sum_{l=1}^{J+J'} f_l^{\varepsilon}(x,t). \end{cases} \tag{35}$$

The Maxwellian function $\mathcal{M}_l$ for the l-th equation of the system is chosen as one of the Maxwellian described in Section 2.2.

In a BGK approximation (3), the minimal number L of discrete velocities depends on the spatial dimension of the problem. For the one-dimensional case we consider $L = 4$ ($J = J' = 2$) possible velocity directions, whereas for the two-dimensional case we set $L = 6$ ($J = J' = 3$). It has been shown that increasing the number of discrete velocities L does not provide better results in terms of accuracy [7] and since the computational complexity for the numerical approximation of the relaxation system clearly depends on the number of velocities, we will take those values $L = 4$ (in the 1D case) and $L = 6$ (in the 2D case) fixed from now on.

2.3.2 Spatial Discretization

The spatial discretization of Equation (35) is performed by treating the advection term alone. Here we detail the approximation for a second-order (and fourth-order) finite volume scheme, but this can be easily extended to higher order methods. In particular, as we will observe in Section 3.2, we need a central finite volume scheme for the approximation of the last J' equations.

Assuming a cartesian grid of the form $[0, X_{\max}] \times [0, Y_{\max}]$ for the two-dimensional case, we discretize by considering volumes of size Δx^2 (we automatically assume that $X_{\max}/\Delta x$ and $Y_{\max}/\Delta x$ are integers). Since the kinetic formulations described above consist of decoupled equations along each direction, we restrict to a spatial discretization based on finite volume method in the one-dimensional case, considering a spatially uniform grid. The domain $[0, X_{\max}]$ is divided in I cells $\mathcal{C}_i = [x_{i-1/2}, x_{i+1/2}]$, where $x_{i\pm1/2} = x_i \pm \Delta x/2$ with constant size Δx, over which the cell average of the solution is approximated. A numerical flux function $\mathcal{F}$ is defined to approximate the flux at the interface $x_{i+1/2}$ of each cell, such that the semi-discretized system reads as

$$\frac{d\, f_{l,i}(t)}{dt} = -\frac{1}{\Delta x}\left[\mathcal{F}_{l,i+1/2}(t) - \mathcal{F}_{l,i-1/2}(t)\right], \qquad i = 1, \dots, I \quad l = 1, \dots, L. \tag{36}$$

This provides an approximation $f_{l,i}$ for the cell average of f_l in $\mathcal{C}_i$, where the numerical flux satisfies for the linear advection with constant velocity Γ_l

$$\mathcal{F}_{l,i+1/2}(t) \approx \Gamma_l f_{l,i+1/2}(t), \qquad i = 1, \dots, I \quad l = 1, \dots, L. \tag{37}$$

For the first J equations we consider k-th order upwind scheme, to guarantee the consistency of the scheme with the discrete BGK scheme (3). The numerical flux for a first order upwind scheme could be defined as

$$\mathcal{F}_{l,i+1/2}(t) = \begin{cases} \Gamma_l\, f_{l,i} & \text{if } \Gamma_l > 0, \\ \Gamma_l\, f_{l,i+1} & \text{if } \Gamma_l < 0. \end{cases} \tag{38}$$

Higher order extension of upwind schemes are easily recovered (see for instance [51]). For instance, a third order upwind biased scheme reads as

$$\mathcal{F}_{l,i+1/2}(t) = \begin{cases} \Gamma_l \dfrac{2\, f_{l,i+1} + 3\, f_{l,i} - 6\, f_{l,i-1} + f_{l,i-2}}{6} & \text{if } \Gamma_l > 0, \\ \Gamma_l \dfrac{-2\, f_{l,i+2} + 6\, f_{l,i+1} - 3\, f_{l,i} + f_{l,i-1}}{6} & \text{if } \Gamma_l < 0, \end{cases} \tag{39}$$

for $l = 1, \dots, J$. The fourth order extension is given by the following expression

$$\mathcal{F}_{l,i+1/2}(t) = \begin{cases} \Gamma_l \dfrac{-f_{l,i+2} + 8\, f_{l,i+1} - 8\, f_{l,i-1} + f_{l,i-2}}{12} & \text{if } \Gamma_l > 0, \\ \Gamma_l \dfrac{f_{l,i+3} - 6\, f_{l,i+2} + 18\, f_{l,i+1} - 10\, f_{l,i} - 3\, f_{l,i-1}}{12} & \text{if } \Gamma_l < 0, \end{cases}$$

for $l = 1, \dots, J$.

The last J' equations are instead approximated using a centered numerical flux, in order to guarantee the consistency of the scheme with the diffusive BGK scheme (3). The second-order centered flux scheme is given by

$$\mathcal{F}_{l,i+1/2}(t) = \Gamma_l \frac{f_{l,i+1} + f_{l,i-1}}{2}, \qquad l = J+1, \dots, L. \tag{40}$$

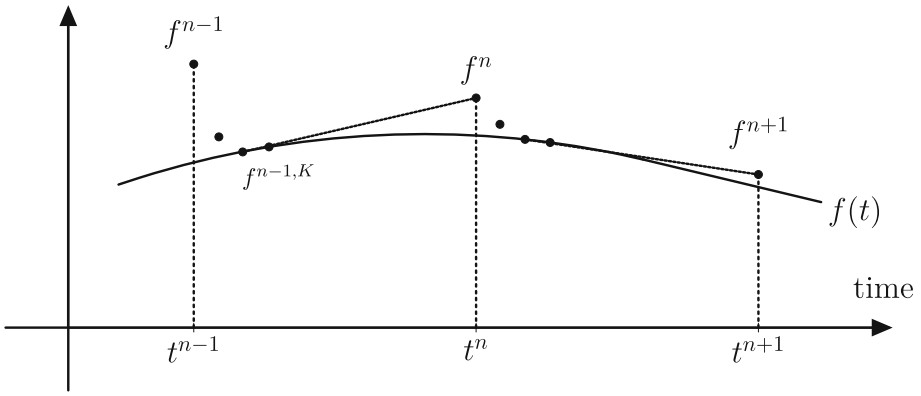

Fig. 1 Idea of Projective Integration method, as sketched in [34]. The numerical solution obtained by explicit integration with small δt is quickly attracted to a slow manifold (solid curve). Then, the solution is projected over a bigger time step Δt through a first order extrapolation

A fourth order extension for centered flux schemes is obtained by considering

$$\mathcal{F}_{l,i+1/2}(t) = \Gamma_l \frac{f_{l,i-2} - 8\, f_{l,i-1} + 8\, f_{l,i+1} - f_{l,i+2}}{12} \qquad l = J+1, \ldots, L.$$

Remark 2 The violation of a maximum principle for a centered flux scheme could lead to unphysical oscillations, which may affect the accuracy in the approximation of the advection equation. However, no additional limiting procedure is required, since the consistency in ε of the kinetic approximation (3) with the advection-diffusion equation (1) quickly stabilizes the oscillations as $\varepsilon \to 0$, as already observed in [34].

3 Projective Integration

The main idea behind the construction of projective integration methods is to combine a few small time steps of a naive (*inner*) time-stepping method, with a projective step (*outer*), in which an extrapolation over a large time interval is performed. The idea is sketched in Fig. 1.

In [34], the authors show how the choice of an outer time step much larger than the inner time step leads to a splitting of the stability region of the method in two circle-like connected components. In that case, the projective integration parameters (magnitude of time steps, number of inner time steps, …) can be taken in order to have all the fast eigenvalues in the first stability region and all the slow (dominant) eigenvalues in the dominant stability region.

Since the main concern for the inner integrator is stability, a natural choice for the inner step is to use a simple, explicit method, such as a forward Euler discretization. For the outer integrator, a higher-order extension of the extrapolation step can be performed in the Runge-Kutta fashion. The first order accuracy of the inner integrator contributes only an $\mathcal{O}(\varepsilon)$ term to the overall error, while the leading error terms are determined by the outer integrator. This approach yields a fully explicit, arbitrary order time integration method for stiff systems, sharing important features with asymptotic-preserving schemes. Indeed, despite the impossibility of evaluating the scheme for $\varepsilon = 0$, the computational cost of this method

is independent from the stiffness of the problem. This implies that it is possible to solve stiff problems without requiring restrictive CFL condition, as done in the series of papers [2, 27, 28, 32, 34, 41] for different stiff kinetic equations. It is worth mentioning extensions of projective integration schemes to problems with multiple time scales known as *telescopic projective integration* schemes, and we refer to [8, 21, 40]. The strategy is based on a hierarchy of projective levels in which the extrapolation procedure is recursively repeated, in order to construct a method with a computational complexity essentially independent of the stiffness of the problem.

The idea is to use the same approach to numerically approximate the BGK approximation (3) in the limit for $\varepsilon \to 0$ with an asymptotic-preserving scheme.

Let us introduce the time step δt and let us consider the classical forward Euler method

$$f^{k+1} = S_{\delta t}(f^k) = f^k + \delta t\, D_t^{\varepsilon}(f^k) \qquad k = 0, 1, \ldots, \tag{41}$$

where D_t^{ε} is given by (34). This is problematic for $\varepsilon \to 0$, since the condition becomes too restrictive and the spatial discretization in the kinetic space may lead unstabilities in the macroscopic space.

When $\varepsilon \to 0$, the system formally converges to a limiting equation for which every finite volume scheme needs to satisfy a weaker stability restriction. The idea of projective integration schemes is to exploit the structure of the kinetic operator to accelerate the integration.

Let us now introduce step sizes δt and Δt, which represent the inner and the outer time steps respectively. Then, the solution $f(t)$ is approximated by $f^{n,k}$ at time $t = n\Delta t + k\delta t$.

Starting from a computed numerical solution f^n at time $t^n = n\Delta t$, one first takes $K + 1$ inner steps of size δt, using as inner integrator the forward Euler method in (41), obtaining

$$f^{n,k+1} = S_{\delta t}(f^{n,k}) = f^{n,k} + \delta t\, D_t^{\varepsilon}(f^{n,k}) \qquad k = 0, 1, \ldots, K, \tag{42}$$

where $f^{n,0} = f^n$. The number K of inner time steps is one of the parameters to be determined.

Then, we approximate the time derivative of f, computing f^{n+1} via extrapolation in time. The last two updates of (42), $f^{n,K}$ and $f^{n,K+1}$ are used to project the solution forward

$$\begin{aligned} f^{n+1} &= f^{n,K+1} + (\Delta t - (K+1)\delta t)\frac{f^{n,K+1} - f^{n,K}}{\delta t} \\ &= f^{n,K+1} + M\delta t \frac{f^{n,K+1} - f^{n,K}}{\delta t}, \end{aligned} \tag{43}$$

in which we have defined the relative size of the extrapolation M as:

$$M = \frac{\Delta t}{\delta t} - (K+1). \tag{44}$$

This method (43) is called *projective forward Euler* (PFE), due to the fact that the extrapolation is performed using a first-order approximation of the derivative.

High-Order Projective Runge-Kutta Methods

It is possible to employ in principle any Runge-Kutta method as inner integrator, replacing each time derivative evaluation in a classical Runge-Kutta method by $K + 1$ steps of an inner integrator, as discussed in [32]. However, the order of the scheme is dominated by the outer integrator. The idea is to use a particular higher order extension of projective integration, based on Runge-Kutta methods. Here, we briefly recall the construction of the projective Runge-Kutta (PRK) method. Using the same coefficients introduced in Appendix A for

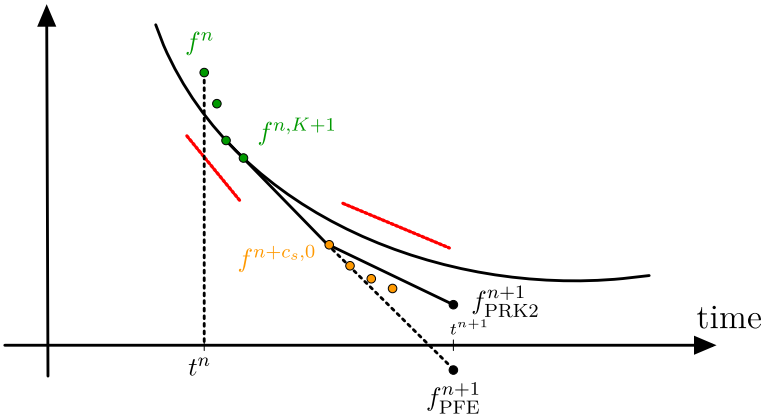

Fig. 2 Idea of the Projective Runge-Kutta Integration method. The scheme first computes $f^{n,K+1}$ through (45), followed by an extrapolation which yields $f^{n+c_s,0}$. Then, $f^{n+c_s,K+1}$ is obtained applying a Runge-Kutta-based approach (46), from which the final solution is recovered via (47)

classical Runge-Kutta methods, for an explicit S-stage PRK scheme, we compute the values $\mathbf{k}_s$ as

$$s = 1 : \begin{cases} f^{n,k+1} = f^{n,k} + \delta t\, D_t(f^{n,k}) & 0 \le k \le K, \\ \mathbf{k}_1 = \dfrac{f^{n,K+1} - f^{n,K}}{\delta t}, \end{cases} \tag{45}$$

$$2 \le s \le S : \begin{cases} f^{n+c_s,0} = f^{n,K+1} + (c_s \Delta t - (K+1)\delta t) \displaystyle\sum_{l=1}^{s-1} \frac{a_{s,l}}{c_s} \mathbf{k}_l, \\ f^{n+c_s,k+1} = f^{n+c_s,k} + \delta t\, D_t(f^{n+c_s,k}) & 0 \le k \le K, \\ \mathbf{k}_s = \dfrac{f^{n+c_s,K+1} - f^{n+c_s,K}}{\delta t}, \end{cases} \tag{46}$$

where $f^{n+c_s,k} \approx f(t^n + c_s\Delta t + k\delta t)$, with $a_{s,l}$ and c_s the *Runge-Kutta matrix* and the *Runge-Kutta nodes*, respectively. Finally, the numerical solution at time t^{n+1} is computed as

$$f^{n+1} = f^{n,K+1} + (\Delta t - (K+1)\delta t) \sum_{s=1}^{S} b_s\, \mathbf{k}_s, \tag{47}$$

where b_s are the *Runge-Kutta weights*. The explicit expression for the coefficients of the Runge-Kutta schemes is given in the Appendix A. In Fig. 2 we sketch the idea of Projective Runge-Kutta schemes for a second order case. Heuristically, each time derivative evaluation k_s is replaced by $K+1$ steps of an inner integrator and a time derivative estimate. This Runge-Kutta based formulation allows a higher order extension of the PFE method.

Remark 3 Despite the order of the scheme is usually dominated by the outer integrators, when using higher order approximation for the outer integrator, it may be useful to introduce high order schemes as inner integrator, too. For instance, a 5th order scheme with $\Delta t = 0.01$ has a consistency error which is $\mathcal{O}(10^{-10})$, thus the error is dominated by the inner integrator whenever a first order approximation is used and $\varepsilon > 10^{-10}$. A second order approximation for the inner integrator typically removes issues of this kind.

Remark 4 A very recent and interesting approach is given in [29], where the authors prove that all existing Projective Integration methods can be written as Runge–Kutta methods with an extended Butcher tableau including many stages. This approach allows to use many tools for stability and consistency analysis of the Runge-Kutta schemes in the framework of Projective Integration.

3.1 Stability Analysis

The main advantage of projective integration approach is its great speed up for problems with large scale separation, but it is fundamental to estimate the spectrum of the inner integrator for the equation to correctly identify the parameters of the PI (Δt, δt and K) and guarantee the stability of the scheme. The estimation of the spectrum for a general BGK operator in the discrete kinetic approximation framework could be extremely hard. For this reason, we propose here an analysis of the spectrum for a simplified setting, namely taking $A(u) = u$ and $B(u) = u$ in (1) and the diagonal relaxation model (DRM1). The generalization of this setting to nonlinear Maxwellians is still an open question and represents an interesting aspect to investigate.

Let us consider the scalar BGK approximation in Equation (16) with a linear Maxwellian in the form of (19)

$$\mathcal{M}_{\lambda,\theta}(u) = \left(u + \frac{u}{\lambda} - \frac{u}{\theta^2},\, u - \frac{u}{\lambda} - \frac{u}{\theta^2},\, \frac{u}{\theta^2},\, \frac{u}{\theta^2}\right). \tag{48}$$

We can rewrite the semidiscrete kinetic equation (34) in the Fourier (spatial) domain as

$$\partial_t \hat{f}(\xi_k) = \mathcal{K}\hat{f}(\xi_k), \qquad \mathcal{K} = \frac{1}{\varepsilon}\left(-\varepsilon D + MP - I\right) \tag{49}$$

where $\hat{f} \in \mathbb{R}^4$, $I \in \mathbb{R}^{4\times 4}$ is the identity matrix, $P \in \mathbb{R}^{4\times 4}$ is the orthogonal projection matrix and $M \in \mathbb{R}^{4\times 4}$ is given by

$$M = \frac{1}{2}\begin{pmatrix} 1 + \frac{1}{\lambda} - \frac{1}{\theta^2} & 0 & 0 & 0 \\ 0 & 1 - \frac{1}{\lambda} - \frac{1}{\theta^2} & 0 & 0 \\ 0 & 0 & \frac{1}{\theta^2} & 0 \\ 0 & 0 & 0 & \frac{1}{\theta^2} \end{pmatrix}. \tag{50}$$

The advection matrix $D \in \mathbb{R}^{4\times 4}$ can be written as

$$D = \begin{pmatrix} \alpha + i\,\beta & 0 & 0 & 0 \\ 0 & \alpha - i\,\beta & 0 & 0 \\ 0 & 0 & \frac{1}{\sqrt{\varepsilon}}(\xi + i\,\gamma) & 0 \\ 0 & 0 & 0 & \frac{1}{\sqrt{\varepsilon}}(\xi - i\,\gamma) \end{pmatrix}. \tag{51}$$

Here D represents the Fourier matrix of the spatial discretisation chosen for the advection term, and α, β are respectively the real and the imaginary part of the upwind approximation. For instance, for the third order upwind scheme, we have

$$\begin{cases} \alpha = -\dfrac{|\lambda|}{6\,\Delta x}\left(3 - 4\cos(\zeta) + \cos(2\zeta)\right), \\ \beta = -\dfrac{\lambda}{6\,\Delta x}(8\,\sin(\zeta) - \sin(2\,\zeta)). \end{cases} \tag{52}$$

Analogously, ξ and γ are respectively the real and the imaginary part of the centered approximation. For instance, for the fourth order central scheme, we have

$$\begin{cases} \xi = 0, \\ \gamma = \left(\dfrac{\mu}{\sqrt{2}} + \dfrac{\theta}{\sqrt{\varepsilon}} \right) \dfrac{8\sin(\zeta) - \sin(2\zeta)}{6\,\Delta x}. \end{cases} \tag{53}$$

Let us define an auxiliary matrix $\mathcal{A} = -\varepsilon\, D + M P$, such that $\mathcal{K} = \varepsilon^{-1}(\mathcal{A} - I)$. Since the matrix has the following structure

$$\mathcal{A} = D + u\, e^T, \tag{54}$$

where e is the canonical vector in $\mathbb{R}^4$, we can use Sherman-Morrison formula to compute the determinant $\chi_{\mathcal{A}}$ [22], which is given by

$$\chi_{\mathcal{A}}(\zeta) = \prod_{i=1}^{4}(-\varepsilon D_i - \zeta) \left(1 + \frac{1}{4} \sum_{j=1}^{4} \frac{M_j}{-\varepsilon D_j - \zeta} \right), \tag{55}$$

where D_i denotes the i-th diagonal entries of D and M_j denotes the j-th diagonal entries of M.

Following [32], it is possible to localize the eigenvalues, by using Rouché's Theorem. The main differences here are given by the non-constant ε-dependency of the coefficients D_j and the non-uniform structure of M_j.

Theorem 1 *The spectrum of the matrix $\mathcal{A}$ satisfies*

$$Sp(\mathcal{A}) \subset \mathcal{D}\left(0, C\sqrt{\varepsilon}(|\xi| + |\gamma|)\right) \cup \{\zeta(\varepsilon)\}, \tag{56}$$

where C is a constant depending on the entries of D, ξ and γ are defined in (51) and $\zeta(\varepsilon)$ is the dominant eigenvalue.

For the sake of completeness we retrace the proof of Theorem 1 in the Appendix B, extending the results in [32, Theorem 4.1]. As a consequence, the spectrum of $\mathcal{K}$ satisfies

$$\mathrm{Sp}\,(\mathcal{K}) \subset \left(\mathcal{D}\left(-\frac{1}{\varepsilon}, C\,\frac{1}{\sqrt{\varepsilon}}\,(|\xi| + |\gamma|) \right) \right) \cup \{\zeta(\varepsilon)\}, \tag{57}$$

where ζ is the dominant eigenvalue, whose explicit expression, in the case of the third order upwind scheme (52) for the hyperbolic part and the fourth order centered scheme (53) for the parabolic part, is given by

$$\begin{cases} \mathrm{Re}\,(\zeta(\varepsilon)) = \left(1 - \dfrac{1}{\theta^2}\right) \alpha + \mathcal{O}(\varepsilon), \\ \mathrm{Im}\,(\zeta(\varepsilon)) = \dfrac{\beta}{\lambda} + \mathcal{O}(\varepsilon). \end{cases} \tag{58}$$

We first observe that the spectrum of $\mathcal{K} = \varepsilon^{-1}\,(\mathcal{A} - I)$ consists of two well separated clusters for $\varepsilon \to 0$ and its localization on the real axis is given by two contributions: the dominant eigenvalue, whose real part is $\mathcal{O}(1)$, and the remaining eigenvalues, contained in a region around $-1/\varepsilon$. This is consistent with the derivation of the spectrum eigenvalues for a linearized BGK operator, as shown in [17].

Moreover, we assess our theoretical result by introducing a numerical approximation of the spectrum, as done in [8].

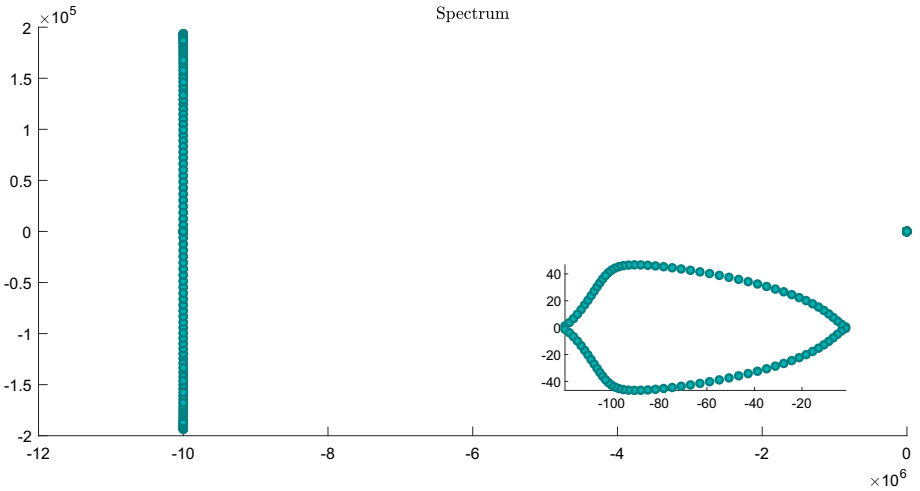

Fig. 3 Spectrum of the operator $\mathcal{K}$ for $\varepsilon = 10^{-7}$

By introducing a finite volume approximation of the phase space and implementing, for instance, the forward Euler time discretization of (33), the semidiscrete operator could be rewritten as

$$G(f^{n,k}) = \frac{F(f^{n,k}) - f^{n,k}}{\delta t}, \tag{59}$$

where $F(f^{n,k}) = f^{n,k+1}$. The function $G(f^{n,k})$ represents the discretization of the temporal derivative, which, according to (33), gives us a discrete approximation of D_t^{ε}. The Jacobian of this operator and its eigenvalues can be now computed numerically, to obtain a numerical approximation of the spectrum of our problem.

In Fig. 3 we show the spectrum of the operator for $\varepsilon = 10^{-7}$ with a central difference scheme for the parabolic terms, choosing $\delta t = \varepsilon$. Similarly to the spectrum of a BGK equation in the diffusive scaling, here the imaginary part is governed by $\sqrt{\varepsilon}$, in accordance to (57).

In [20] it has been shown that the stability region of the PFE consists of the union of two separated disks $\mathcal{D}_1^{\text{PFE}} \cup \mathcal{D}_2^{\text{PFE}}$, where

$$\mathcal{D}_1^{\text{PFE}} = \mathcal{D}\left(1 - \frac{\delta t}{\Delta t}, \frac{\delta t}{\Delta t}\right), \qquad \mathcal{D}_2^{\text{PFE}}\left(0, \left(\frac{\delta t}{\Delta t}\right)^{\frac{1}{K}}\right), \tag{60}$$

and $\mathcal{D}(c, r)$ denotes the ball with center $(c, 0)$ and radius r in the complex λ-plane. The eigenvalues lying in $\mathcal{D}_1^{\text{PFE}}$ correspond to the slowly decaying modes, whereas the eigenvalues $\mathcal{D}_2^{\text{PFE}}$ correspond to the fast modes, quickly damped by the inner integrator. Since the dominant set of eigenvalues is given by $\mathcal{D}_1^{\text{PFE}}$, the approach of projective integration schemes is to suitably choose the method parameters δt, Δt and K to allow for accurate integration of the modes in $\mathcal{D}_1^{\text{PFE}}$, while ensuring stability for the modes in $\mathcal{D}_2^{\text{PFE}}$.

Let us recall that the Fourier transform of the inner forward Euler scheme is given by

$$\hat{F}^{k+1} = (I + \delta t \mathcal{K})\, \hat{F}^k, \tag{61}$$

which means that the spectrum satisfies

$$\mathrm{Sp}\,(I+\delta t\mathcal{K}) = \left(\mathcal{D}\left(1-\frac{\delta t}{\varepsilon}, C\,\frac{\delta t}{\sqrt{\varepsilon}}\,(|\xi|+|\gamma|)\right)\right)\cup\{1+\delta t\,\zeta(\varepsilon)\}\,. \tag{62}$$

From a heuristic standpoint, the stability of the method can be ensured by requiring that the stability region defined in Equation (60) encompasses the spectrum derived in Equation (62). In [32], it has been shown that the choice of stable parameters for the PFE guarantees also the stability of high order projective integration methods, since the higher-order stability domains include the PFE one. Thus, according to Theorem 1 , the spectrum (62) and the stability region (60), we set the parameters for projective integration method as follows:

$$\delta t = \varepsilon, \qquad K \geq 2. \tag{63}$$

The Δt is chosen according to the diffusive CFL condition, namely $\Delta t = C\Delta x^2$. In the following we set

$$\Delta t \leq \frac{\Delta x^2}{2\theta^2}. \tag{64}$$

We refer to the Appendix C for a detailed description of the stability analysis of PRK schemes.

3.2 Consistency Analysis

The consistency analysis for our numerical method is performed again in the scalar one-dimensional setting, following the derivation in [34]. For this purpose, we consider the expression (8). The scheme is given by

$$f^{n+1} = S_{\delta t} f^n = f^n + \delta t\left(-\Phi^{\varepsilon}(f^n) + \frac{\mathcal{M}(u^n) - f^n}{\varepsilon}\right), \tag{65}$$

where Φ^{ε} is the spatial discretization operator.

If we consider $\delta t = \varepsilon$ (according to the stability condition) and a centered flux for the last J' equations, the inner scheme is then reduced to the following expression

$$f^{n+1} = S_{\varepsilon} f^n = \mathcal{M}(u^n) - \varepsilon\Phi^{\varepsilon}(f^n). \tag{66}$$

The corresponding density u^{N+1} at time t^{N+1} satisfies

$$u^{N+1} = u^{N,K+1} + (\Delta t - (K+1)\varepsilon)\,\frac{u^{N,K+1} - u^{N,K}}{\varepsilon}, \tag{67}$$

where $K+1$ is the number of inner time steps taken to guarantee the stability of the method.

The truncation error could be defined for the macroscopic quantities as

$$E^{N+1} = \frac{\tilde{u}^{N+1} - u^{N+1}}{\Delta t}, \tag{68}$$

where $\tilde{u}^N$ is the exact solution for u at time t^N.

By considering the projective step, we can rewrite the truncation error as

$$E^{N+1} = \frac{\tilde{u}^{N+1} - u^{N,K+1}}{\Delta t} - \left(\frac{\Delta t - (K+1)\varepsilon}{\Delta t}\right)\frac{u^{N,K+1} - u^{N,K}}{\varepsilon}. \tag{69}$$

This means that the local truncation error of the projective scheme depends on its inner integrator too. Thus, we introduce the local truncation error of the inner integrator related to

the kinetic variable f as

$$e_f^{N,k+1} = \frac{\tilde{f}^{N,k+1} - f^{N,k+1}}{\delta t} = \frac{\tilde{f}^{N,k+1} - f^{N,k+1}}{\varepsilon}. \tag{70}$$

We can rewrite both quantities in terms of their solution at time $t^{N,k}$. For $f^{N,k+1}$ we simply use the expression of the inner integrator, which, in this case, is chosen as the Forward Euler scheme

$$f^{N,k+1} = S_\varepsilon f^{N,k} = \mathcal{M}(u^{N,k}) - \varepsilon \Phi^\varepsilon(f^{N,k}). \tag{71}$$

The exact solution $\tilde{f}^{N,k+1}$ is expanded through a Taylor series around $t^{N,k}$, using the kinetic formulation of the model (3)

$$\begin{aligned} \tilde{f}^{N,k+1} &= \tilde{f}^{N,k} + \varepsilon \partial_t \tilde{f}^{N,k} + \mathcal{O}(\varepsilon^2) \\ &= \tilde{f}^{N,k} - \varepsilon \left(\Gamma \partial_x \tilde{f}^{N,k} \right) + \left(\mathcal{M}(\tilde{u}^{N,k}) - \tilde{f}^{N,k} \right) + \mathcal{O}(\varepsilon^2) \\ &= S_\varepsilon(\tilde{f}^{N,k}) + \varepsilon \left(\Phi^\varepsilon(\tilde{f}^{N,k}) - \Gamma \partial_x \tilde{f}^{N,k} \right) + \mathcal{O}(\varepsilon^2). \end{aligned} \tag{72}$$

The third equality is obtained from adding and subtracting $\Phi^\varepsilon(\tilde{f}^{N,k})$ to the expression and using the forward Euler operator S_ε.

This leads to

$$e_f^{N,k+1} = S_\varepsilon(e_f^{N,k}) + \left(\Phi^\varepsilon(\tilde{f}^{N,k}) - \Gamma \partial_x \tilde{f}^{N,k} \right) + \mathcal{O}(\varepsilon). \tag{73}$$

By recursion, recalling that $e^{N,0} = 0$, we can rewrite

$$e_f^{N,K+1} = \sum_{k=0}^{K} S_\varepsilon^k \left(\Phi^\varepsilon(\tilde{f}^{N,K-k}) - \Gamma \partial_x \tilde{f}^{N,K-k} \right) + \mathcal{O}((K+1)\varepsilon). \tag{74}$$

Let us split the expression as

$$\begin{aligned} e_f^{N,K+1} = \sum_{k=0}^{K} S_\varepsilon^k \Bigg[& \mathcal{A}(\tilde{f}^{N,K-k}) - \sum_{j=1}^{J} \lambda_j \partial_x \tilde{f}^{N,K-k} \\ & + \left(\frac{\mu}{\sqrt{2}} + \frac{\theta}{\sqrt{\varepsilon}} \right) \left(\mathcal{B}(\tilde{f}^{N,K-k}) - \sum_{j=J+1}^{J'} \partial_x \tilde{f}^{N,K-k} \right) \Bigg] + \mathcal{O}((K+1)\varepsilon), \end{aligned} \tag{75}$$

where $\mathcal{A}$ is the spatial upwind discretization operator corresponding to the hyperbolic term and $\mathcal{B}$ is the spatial centered flux discretization operator corresponding to the parabolic term.

The difference inside the brackets in equation (75) precisely corresponds to sum of the spatial discretization error related to the hyperbolic contribution and the one related to the parabolic contribution. Unfortunately, if we compute directly the spatial truncation error using a centered scheme for the parabolic terms, a term $\Delta x^2/\sqrt{\varepsilon}$ appears. Following the idea of [34], let us estimate explicitly $S_\varepsilon \Delta f$, where

$$\begin{aligned} \Delta : f^\varepsilon \in C_c^\infty \left(\Omega \times (0,T);\, \mathbb{R}^L \right) \mapsto & \mathcal{A}(f^\varepsilon) - \sum_{j=1}^{J} \lambda_j \partial_x f^\varepsilon \\ & + \left(\frac{\mu}{\sqrt{2}} + \frac{\theta}{\sqrt{\varepsilon}} \right) \left(\mathcal{B}(f^\varepsilon) - \sum_{j=J+1}^{J'} \operatorname{sign}(\gamma_j) \partial_x f^\varepsilon \right). \end{aligned}$$

For the sake of simplicity we also define the corresponding operators

$$\Delta_{\mathcal{A}} : f^\varepsilon \in C_c^\infty\left(\Omega \times (0,T);\, \mathbb{R}^L\right) \mapsto \mathcal{A}(f^\varepsilon) - \sum_{j=1}^{J} \lambda_j \partial_x f^\varepsilon,$$

$$\Delta_{\mathcal{B}} : f^\varepsilon \in C_c^\infty\left(\Omega \times (0,T);\, \mathbb{R}^L\right) \mapsto \left(\frac{\mu}{\sqrt{2}} + \frac{\theta}{\sqrt{\varepsilon}}\right)\left(\mathcal{B}(f^\varepsilon) - \sum_{j=J+1}^{J'} \operatorname{sign}(\gamma_j)\partial_x f^\varepsilon\right).$$

Then, we can rewrite (66) as

$$S_\varepsilon(\Delta f^\varepsilon) = \mathcal{M}\left(\sum_i \Delta f_i^\varepsilon\right) - \varepsilon\, \Phi\, \Delta\, f^\varepsilon, \tag{76}$$

where we recall the linearity of the Maxwellian functions $\mathcal{M}$. Consequently, we have

$$S_\varepsilon^2(\Delta f^\varepsilon) = \mathcal{M}\left(\sum_i \Delta f_i^\varepsilon\right) - \varepsilon\, \mathcal{M}\left(\sum_i \Phi\, \Delta\, f_i^\varepsilon\right) - \varepsilon \Phi \mathcal{M}\left(\sum_i \Delta f_i^\varepsilon\right) + \varepsilon^2 \Phi^2 \Delta f^\varepsilon, \tag{77}$$

which yields, for $k \geq 3$

$$\begin{aligned} S_\varepsilon^k(\Delta_\Phi f^\varepsilon) = {} & \mathcal{M}\left(\sum_i \Delta f_i^\varepsilon\right) - \varepsilon\, \mathcal{M}\left(\sum_i \Phi^\varepsilon\, \Delta\, f_i^\varepsilon\right) - \varepsilon \Phi^\varepsilon \mathcal{M}\left(\sum_i \Delta f_i^\varepsilon\right) \\ & + \varepsilon(k-2)\mathcal{M}\left(\Phi^\varepsilon \mathcal{M}\left(\sum_i \Delta f_i\right)\right) + \mathcal{O}(\varepsilon^2). \end{aligned} \tag{78}$$

Let us now compute the average value of $S_\varepsilon^k(\Delta f^\varepsilon)$. Please observe that the hyperbolic contribution has a spatial truncation error given to the second order upwind approximation, which corresponds to $\mathcal{O}(\Delta x^2)$. In particular, we observe that

$$f_i^\varepsilon = \mathcal{M}_i\left(\sum_j f_j^\varepsilon\right) + \sqrt{\varepsilon} g_i^\varepsilon, \qquad i = J+1, \ldots, J',$$

and that $\Delta_{\mathcal{B}}$ is odd in the velocity space.
For $k = 0$,

$$\sum_i \Delta f_i^\varepsilon = \sum_{j=1}^{J} \Delta_{\mathcal{A}} f_j^\varepsilon + \sqrt{\varepsilon} \sum_{j=J+1}^{J'} \Delta_{\mathcal{B}} g_j^\varepsilon = \mathcal{O}(\Delta x^2), \tag{79}$$

since $\Delta_{\mathcal{B}} g_j^\varepsilon = \mathcal{O}(\Delta x^2/\sqrt{\varepsilon})$. For $k = 1$,

$$\begin{aligned} \sum_i S_\varepsilon(\Delta f_i^\varepsilon) &= \sum_{j=1}^{J} \Delta_{\mathcal{A}} f_j^\varepsilon + \sqrt{\varepsilon} \sum_{j=J+1}^{J'} \Delta_{\mathcal{B}} g_j^\varepsilon - \varepsilon \sum_{j=1}^{J} \mathcal{A}\Delta_{\mathcal{A}} f_j^\varepsilon - \varepsilon^{3/2} \sum_{j=J+1}^{J'} \mathcal{B}\Delta_{\mathcal{B}} g_j^\varepsilon + \mathcal{O}(\varepsilon^2) \\ &= \mathcal{O}(\Delta x^2) + \varepsilon \mathcal{O}(\Delta x^2) + \mathcal{O}(\varepsilon^2). \end{aligned}$$

More generally, for $k \geq 2$, we obtain

$$\sum_i S_\varepsilon^k(\Delta_{\mathcal{B}} f_i^\varepsilon) = \mathcal{O}(\Delta x^2) + \varepsilon \mathcal{O}(\Delta x^2) + \mathcal{O}(\varepsilon^2). \tag{80}$$

The last estimate together with Young's inequality plugged in (75) leads to

$$e_i^{N,K+1} = \mathcal{O}\left((K+1)\Delta x^2\right) + \mathcal{O}\left((K+1)\varepsilon\right), \qquad \forall\, K \geq 1, \tag{81}$$

where the contribution comes from (80). This implies that

$$\begin{aligned} E^{N+1} =& \frac{\tilde{u}^{N+1} - u^{N,K+1} + \varepsilon \sum_i e_i^{N,K+1}}{\Delta t} - \left(1 - (K+1)\frac{\varepsilon}{\Delta t}\right) \frac{\tilde{u}^{N,K+1} - \tilde{u}^{N,K}}{\varepsilon} \\ & - \left(1 - (K+1)\frac{\varepsilon}{\Delta t}\right) \sum_i \left(e_i^{N,K+1} - e_i^{N,K}\right) \\ =& \left(1 - (K+1)\frac{\varepsilon}{\Delta t}\right) \partial_t u(t^{N,K+1}) + \mathcal{O}(\Delta t) + \varepsilon \mathcal{O}\left(\frac{\Delta x^2 + \varepsilon}{\Delta t}\right) \\ & - \left(1 - (K+1)\frac{\varepsilon}{\Delta t}\right) \partial_t u(t^{N,K+1}) + \mathcal{O}(\varepsilon) \\ & + \mathcal{O}(\Delta x^2) + \mathcal{O}(\varepsilon) + \mathcal{O}\left(\frac{\varepsilon\, \Delta x^2}{\Delta t}\right) + \mathcal{O}\left(\frac{\varepsilon^2}{\Delta t}\right). \end{aligned} \tag{82}$$

In conclusion, we summarize the above results on consistency of the method:

Theorem 2 *The PFE scheme with second order upwind flux for f_i with $i = 1, \ldots, J$ and centered flux for f_j with $j = J+1, \ldots, L$ is consistent with (3) at order 1 in ε and, as $\varepsilon \to 0$, the limiting scheme is consistent at order 1 in time and 2 in space with (1), namely*

$$E^N = \mathcal{O}(\varepsilon) + \mathcal{O}(\Delta t) + \mathcal{O}(\Delta x^2) + \mathcal{O}\left(\frac{\varepsilon^2}{\Delta t}\right) \overset{\varepsilon \to 0}{\to} \mathcal{O}(\Delta t) + \mathcal{O}(\Delta x^2). \tag{83}$$

In the limit $\varepsilon \to 0$, following the diffusive CFL condition $\Delta t = \mathcal{O}(\Delta x^2)$ we get

$$E^N = \mathcal{O}(\Delta x^2). \tag{84}$$

Remark 5 The extension of this consistency analysis to PRK schemes can be performed by reformulating them as Runge-Kutta schemes [29] and observing that a PRK scheme trivially satisfies RK conditions.

4 Numerical Simulations

In all our numerical simulations, the BGK applied is the DRM1 (19) or the DRM2 (24). We set $\theta = \lambda$ and $\mu = \sqrt{2}\lambda$ unless otherwise mentioned. For the spatial discretization we employ a 4th order upwind scheme combined with a 4th order centered scheme, and for the time discretization we use a PRK4 method, unless otherwise mentioned.

Since the convergence is proven to be $\mathcal{O}(\sqrt{\varepsilon})$, the smaller is ε taken, the better approximation is obtained. For this reason, we set $\varepsilon = 10^{-7}$ in all our numerical simulations.

4.1 Order of Convergence: Linear Diffusion Equation

The test for the order of convergence is first performed for the DRM1 kinetic model by considering the linear diffusion problem [52]

$$\partial_t u = \xi\, \partial_{xx} u, \tag{85}$$

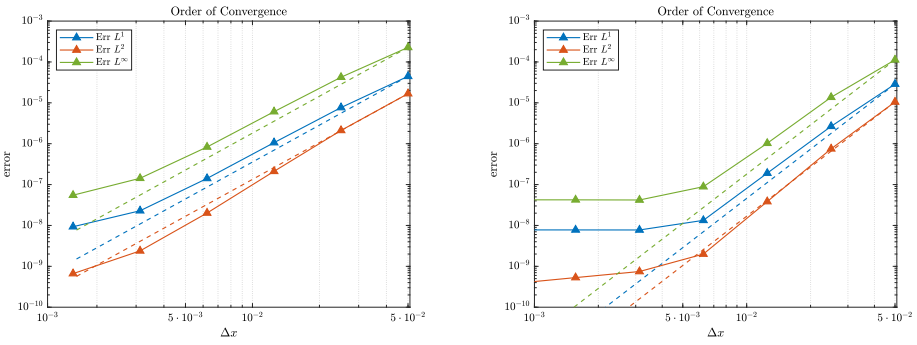

Fig. 4 Spatial order of convergence for the 3rd order scheme (on the left) and the 4th order scheme (on the right) for different norms, using the linear diffusion equation (85). On each plot the solid lines represent the numerical error whereas the dotted line shows the expected error

where $\xi = 10^{-2}$ and the initial condition is u_0, on $(0,\, T) \times \Omega = (0,\, T) \times [0,\ 1]$. In particular, we consider as initial condition

$$u_0(x) = 1 + 0.01 \exp\left(-\frac{(x-0.5)^2}{\delta^2}\right), \tag{86}$$

where $\delta = 0.1$ and with periodic boundary conditions. We compare the numerical solution with the exact solution

$$u(x,t) = 1 + 0.01\sqrt{\frac{\delta^2}{\delta^2 + 4\xi\, t}}\, \exp\left(-\frac{(x-0.5)^2}{\delta^2 + 4\xi\, t}\right). \tag{87}$$

We first test the spatial order of convergence, where the time step is taken equal to $\Delta t = 10^{-7}$ and $\delta t = \varepsilon = 10^{-10}$. With this choice, we are able to study the decrease of the error with respect to the spatial step size Δx (since the truncation error due to the temporal discretization becomes negligible). In Fig 4 we compare the order of convergence in L^1, L^2 and L^∞ norm of the 3rd order scheme and 4th order scheme, plotting the computed error against the expected error in log-log scale. The truncation error behaves as $\mathcal{O}(\Delta x^3)$ and $\mathcal{O}(\Delta x^4)$, respectively, for large Δx, until a plateau is reached. Indeed, for small values of Δx, the contribution of the inner integrator $\mathcal{O}(\varepsilon)$ becomes dominant. This is clearly seen in the 4th order approximation, where the error does not decrease more than 10^{-10}, which corresponds to ε in this test case.

The temporal order of projective integration method is proven using a different approach. Indeed, since we have to satisfy the diffusive CFL condition $\Delta t = \mathcal{O}(\Delta x^2)$, the contribution of the spatial discretization error is dominant. Our idea is based on Richardson extrapolation [29, 50], where two solution computed with different time step $\frac{\Delta t}{k}$, for $k \in \mathbb{N}$ are compared.

Assuming a time discretization of order p, the solution $u^{n+1}_{\Delta t/k}$ is deviating from the exact solution u^{n+1}_* of the semidiscrete system (34) according to

$$u^{n+1}_{\Delta t/k} = u^{n+1}_* + k\, C_n \left(\frac{\Delta t}{k}\right)^{p+1} + \mathcal{O}\left(\Delta t^{p+2}\right), \tag{88}$$

where C_n is the error constant. Therefore, we can rewrite the solution u^{n+1}_* as

$$u^{n+1}_* = \frac{u^{n+1}_{\Delta t} - 2^p u^{n+1}_{\Delta t/2}}{1 - 2^p}, \tag{89}$$

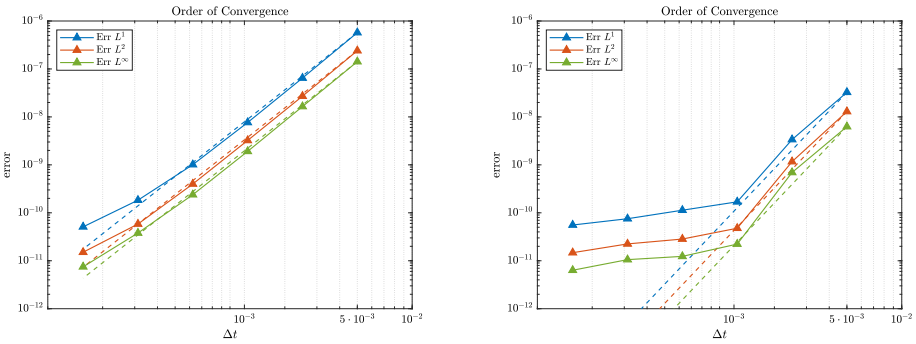

Fig. 5 Temporal order of convergence for the PRK3 (on the left) and the PRK4 (on the right) for different norms, using the linear diffusion equation (85). On each plot the solid lines represent the numerical error whereas the dotted line shows the expected error

from which we obtain an estimation of $u^{n+1}_{\Delta t} - u^{n+1}_*$ in terms of $u^{n+1}_{\Delta t} - u^{n+1}_{\Delta t/2}$, namely

$$u^{n+1}_{\Delta t} - u^{n+1}_* = \frac{2^p \left(u^{n+1}_{\Delta t} - u^{n+1}_{\Delta t/2}\right)}{2^p - 1}. \tag{90}$$

Since to compute the order of convergence we are interested in the ratio between two "consecutive" errors, i.e. errors computed with $\Delta t/k$ and $\Delta t/(2k)$, we can give the following definition of the relative error for a general norm at time T

$$e_{\Delta t} = ||u_{\Delta t}(T) - u_{\Delta t/2}(T)||. \tag{91}$$

One observes that the truncation error behaves as expected and the results are depicted in Fig. 5, where plot the slope of the expected error n log-log scale. In this case, as for the spatial discretization error, the truncation error reaches a plateau, since the contribution of the inner integrator $\mathcal{O}(\varepsilon)$ becomes dominant.

4.2 Order of Convergence: Advection-Diffusion Equation

Following again [52], we propose a test for the advection-diffusion equation with constant velocity c

$$\partial_t u + c\partial_x u = \partial_{xx} u, \tag{92}$$

with the same initial condition as (86). The choice for the discretization parameters is analogous to the previous test. Setting $c = 10$, we reproduce the same test case, where now the solution is advected with a positive velocity. We first test again the spatial order of convergence, in the same setting of the previous case. In Fig. 6 we compare again the order of convergence in L^1, L^2 and L^∞ norm of the 3rd order and 4th order schemes, plotting the computed error against the expected error in log-log scale.

The temporal order of convergence is tested again using the definition in (91). In Fig. 7 we report the slope of the expected error in log-log scale. Differently from the previous test, the plateau is not reached here, since the spatial or the temporal error is dominant compared to the contribution of the inner integrator $\mathcal{O}(\varepsilon)$.

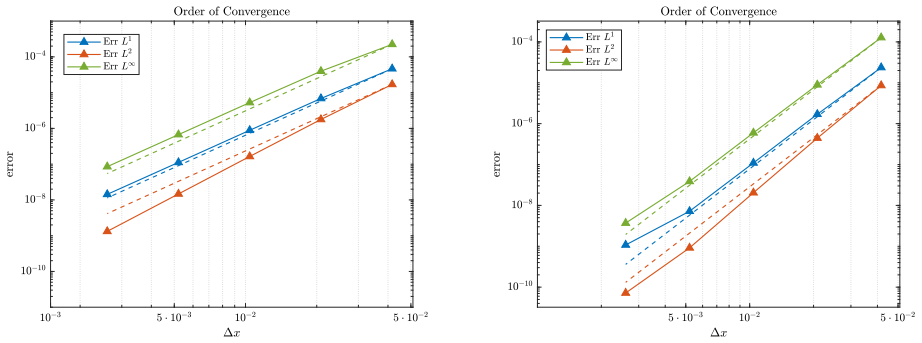

Fig. 6 Spatial order of convergence for the 3rd order scheme (on the left) and the 4th order scheme (on the right) for different norms, using the advection-diffusion equation (85). On each plot the solid lines represent the numerical error whereas the dotted line shows the expected error

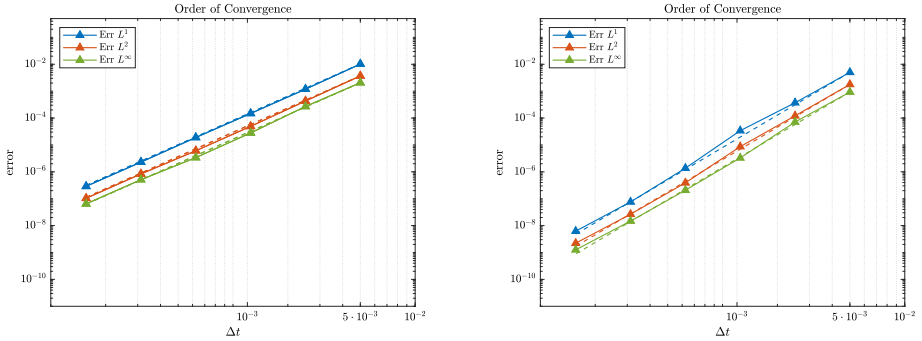

Fig. 7 Temporal order of convergence for the PRK3 (on the left) and the PRK4 (on the right) for different norms, using the advection-diffusion equation (85). On each plot the solid lines represent the numerical error whereas the dotted line shows the expected error

4.3 Testing the Speedup: The Viscous LWR Equation

Let us consider the viscous LWR equation

$$\partial_t u + \partial_x \left(\frac{u - u^2}{2} \right) = \xi \, \partial_{xx} \, u, \tag{93}$$

where ξ assumed different values. We consider the following initial condition, as in [19]

$$u_0(x) = 0.6 + 0.25 \, \sin(2\,\pi \, x), \tag{94}$$

in the domain $[0, 1]$ with periodic boundary conditions and we set the final time $T = 0.13$. The discretization is performed using $\Delta x = 5 \cdot 10^{-3}$ and Δt according to the diffusive CFL condition (64). The projective integration parameters are $\delta t = \varepsilon$ and $K = 2$, where $\varepsilon = 10^{-7}$ from now on. In Fig. 8 we report the solution for $\xi = 10^{-2}$ and $\xi = 10^{-3}$. Let us now test the speedup of the numerical approximation for this test case. From a theoretical point of view, if we assume that the overhead due to extrapolation is negligible and time stepping with the innermost integrator is computationally most demanding, the speedup can be computed as [8, 21, 40]

$$\mathcal{S}_{\text{PI}} = \frac{\Delta t}{\delta t (K + 1)}, \tag{95}$$

Table 1 CPU time (in seconds) and improvement factor

ε	CPU time (s)		Improvement factor	
	Direct	Projective Integration	Real	Theoretical
10^{-5}	1.51	0.89	1.69	1.70
10^{-7}	152	0.94	162	171

Table 2 Comparison between the performance of PFE and first order IMEX scheme

ε	CPU time (s)	
	Projective Integration	IMEX Scheme
10^{-5}	0.89	0.73
10^{-7}	0.94	0.62

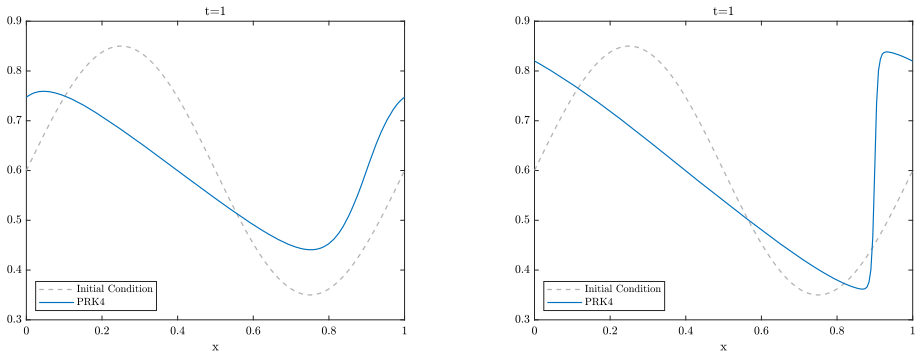

Fig. 8 Numerical approximation of the viscous LWR equation for two different values of ξ, respectively $\xi = 10^{-2}$ (on the left) and $\xi = 10^{-3}$ (on the right)

that is the ratio of the total number of naive forward Euler time steps within one outermost time step over the number of real innermost steps in the method. In Table 1 we report the CPU time of the projective integration method, compared to the classical explicit integration. When $\varepsilon \to 0$, the projective integration approach becomes much more efficient than the direct integration. We compare the theoretical improvement factor (95) with the real improvement factor computed as the ratio between the CPU times.

Moreover, in Table 2 we compare a PFE method with a first order IMEX scheme for stiff BGK equation proposed in [48]. The numerical scheme based on projective integration method exhibits a computational cost of the same order of the IMEX approach (although slightly slower) and it proves to be *asymptotic preserving* with respect to ε. The great advantage of the projective integration approach is that high order extension though a PRK scheme (45)-(46) is easily constructed.

4.4 The Viscous Burgers' Equation

Let us consider the viscous Burgers' equation

$$\partial_t u + \partial_x \left(\frac{1}{2} u^2 \right) = \xi \, \partial_{xx} u, \tag{96}$$

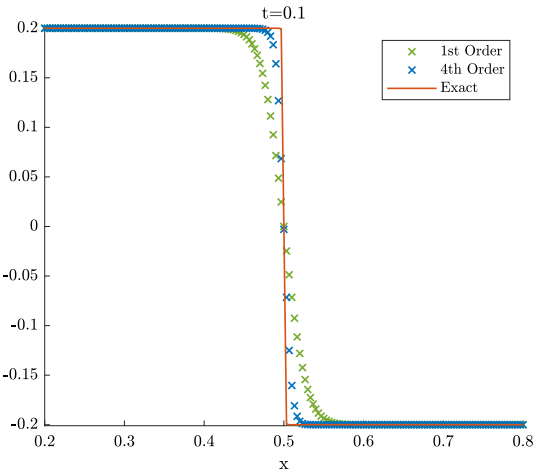

Fig. 9 Comparison of $1st$ order and $4th$ order approximation of the "steady shock" solution to the viscous Burgers' equation (97) with $\Delta x = 3 \cdot 10^{-3}$

where $\xi = 10^{-3}$. We first test our method for the "steady shock" whose exact solution is given by [9, 53]

$$u(x) = -\frac{2\,\xi}{\delta}\,\tanh\left((x - 0.5)/\delta\right), \tag{97}$$

where $\delta = 0.01$. In Fig. 9 we show the results obtained as numerical approximation with schemes of different order. The discretization is performed with step size $\Delta x = 3 \cdot 10^{-3}$ and Δt is chosen according to the diffusive CFL condition (64). The projective integration parameters are chosen as $\delta t = \varepsilon$ and $K = 2$ projective levels. Despite the scheme is not steady-state preserving by construction as in [10], compared to first-order approximation, fourth order PRK4 scheme is able to reduce numerical dissipation errors, well capturing the steady state. The simulation has a perfect agreement with [53].

4.5 The Viscous Burgers' Equation with Strongly Degenerate Diffusion

Let us consider the Burgers equation

$$\partial_t u + \partial_x(u^2) = \xi\,\partial_x\left(\nu(u)\partial_x u\right), \tag{98}$$

with strongly degenerate diffusion

$$\nu(u) = \begin{cases} 0, & |u| \le 0.25, \\ 1, & |u| > 0.25, \end{cases} \tag{99}$$

and the following initial condition

$$u_0(x) = \begin{cases} 1, & \text{if } -\dfrac{1}{\sqrt{2}} - 0.4 \le x \le -\dfrac{1}{\sqrt{2}} + 0.4, \\ -1, & \text{if } \dfrac{1}{\sqrt{2}} - 0.4 \le x \le \dfrac{1}{\sqrt{2}} + 0.4, \\ 0, & \text{otherwise.} \end{cases} \tag{100}$$

We set $\xi = 0.1$ and the discretization parameters are chosen $\Delta x = 0.015$, $\delta t = \varepsilon = 10^{-7}$, $K = 2$ and Δt chosen according to the CFL condition (64). In Fig. 10 we show the numerical

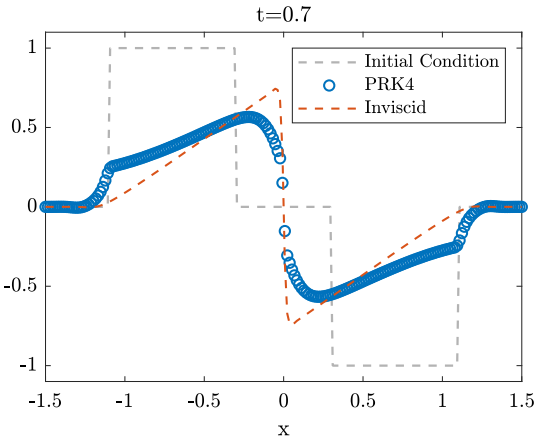

Fig. 10 Numerical approximation of the viscous Burgers' equation compared with the inviscid solution at final time $T = 0.7$ with $\Delta x = 0.015$ and $\xi = 0.1$

results at final time $T = 0.7$, compared with the inviscid case ($\xi = 0$). This test shows the ability of the scheme to deal with strong degenerate diffusions.

4.6 The Two-Dimensional Viscous Burgers' Equation

We propose here an extension of (98) to higher dimensions. Let us focus on the 2D viscous Burgers' equation, explicitly written as

$$\partial_t u + \partial_x \left(u^2\right) + \partial_y \left(u^2\right) = \xi \partial_x \left(\nu(u)\partial_x u\right) + \xi \partial_y \left(\nu(u)\partial_y u\right), \tag{101}$$

again with $\xi = 0.1$ and strongly degenerate diffusion (99) and initial condition

$$u_0(x, y) = \begin{cases} -1 & \text{if } (x-0.5)^2 + (y-0.5)^2 \leq 0.16, \\ 1 & \text{if } (x+0.5)^2 + (y+0.5)^2 \leq 0.16, \\ 0 & \text{otherwise.} \end{cases} \tag{102}$$

The projective integration parameters are $K = 2$, $\delta t = \varepsilon$ and $\Delta t = 0.8\Delta x^2$. The spatial discretization is obtained using $\Delta x = \Delta y = 0.03$ in the domain $[-1.5, 1.5] \times [-1.5, 1.5]$. The simulation in Fig. 11 shows the good approximation with PRK4 scheme, in which the diffusion only acts for $|u| > 0.25$, dealing also in the two-dimensional case with the strongly degenerate parabolic term. We underline again that a great advantage of discrete kinetic BGK approximation is its feasibility of easily extending the strategy to the multidimensional case without increasing the complexity of the structure of system (3).

4.7 A Three-Phase Flow Model

Let us consider the following three phase flow model introduced in the paper of Karlsen et al. [26] and approximated also in [7] to validate the relaxation scheme. It consists of one dimensional system of advection-diffusion equations modeling a multi-phase flow in a porous medium, which reads as follows

$$\begin{cases} \partial_t u + \partial_x f(u) = \xi \partial_{xx} B(u), \\ \partial_t v + \partial_x g(u, v) = \xi \partial_{xx} B(v), \end{cases} \tag{103}$$

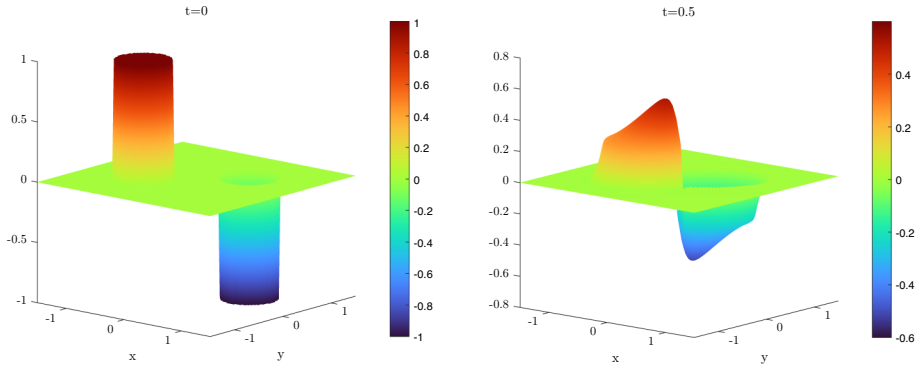

Fig. 11 Numerical approximation of the two-dimensional viscous Burgers' equation: initial condition (left) and final solution at time $t = 0.5$ (right) with $\Delta x = \Delta y = 0.03$ and $\xi = 0.1$

with initial condition given by

$$(u_0(x), v_0(x)) = \begin{cases} (0.4, 0.6), & \text{if } x < 1, \\ (0, 0), & \text{otherwise.} \end{cases} \tag{104}$$

The variables u and v represent the phase saturations (gas and water, respectively), which evolves according to different dynamics. Indeed, the decoupling between the gas phase and the other phase is a reasonable assumption [26] and the flux function $(f(u), g(u, v))$ is given by

$$\begin{cases} f(u) & = \dfrac{u^2}{u^2 + (1-u)^2/10}, \\ g(u, v) & = \dfrac{(1-u)^2 + u^2/10}{10u^2 + (1-u)^2} f(v), \end{cases} \tag{105}$$

and the diffusion function is chosen such that

$$B'(w) = 4w\,(1 - w). \tag{106}$$

The choice of this particular diffusion function is due to the possibility of reproducing the shape of reservoir models. Moreover, we set the scaling factor $\xi = 0.1$ and the relaxation parameter $\varepsilon = 10^{-7}$. In Fig. 12 we show the numerical results for $\Delta x = 0.005$ in $[0, 2.5]$. The projective integration parameters are chosen as $\delta t = \varepsilon$ and $\Delta t = C\Delta x^2$, with $K = 2$ projective levels. The results are in perfect agreement with the one shown in [7]. We observe that the choice of a $4th$ order scheme leads to a less diffusive approximation of the solution, as expected.

We also perform a comparison between DRM1 and DRM2 models, as shown in Fig. 13 with a zoom on the shock. For $\Delta x = 0.05$ the approximation given by the DRM2 model is less dissipative, since the choice of $\lambda_1 \neq -\lambda_2$ improves the kinetic approximation of the original system. Nevertheless, using $\Delta x = 0.0125$, we observe that the two approximations gives equivalent results.

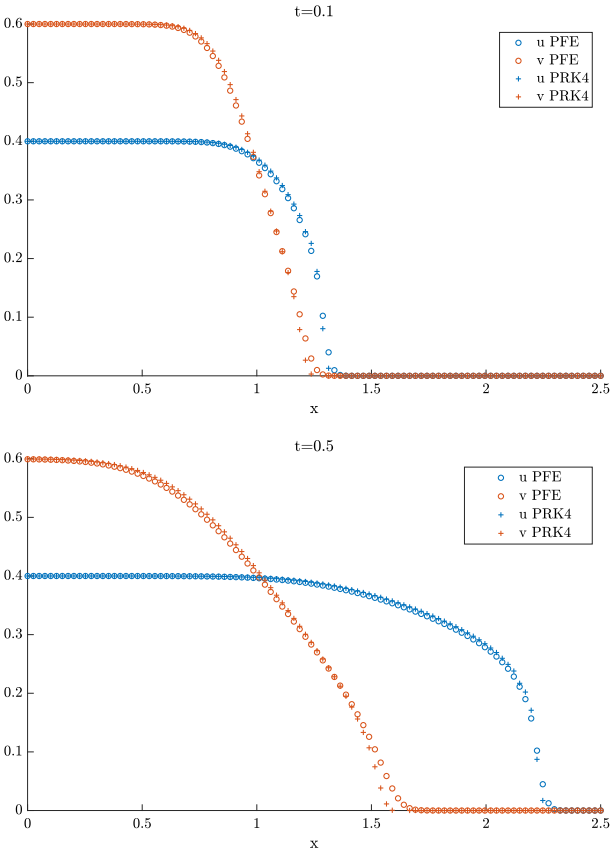

Fig. 12 Numerical approximation of the Buckley-Leverett equation with diffusion for the two phase saturations: gas (in blue) and water (in orange). The evolution of the solution computed with $\Delta x = 0.005$ is shown for two different time frames: $t = 0.1$ (top) and $t = 0.5$ (bottom)

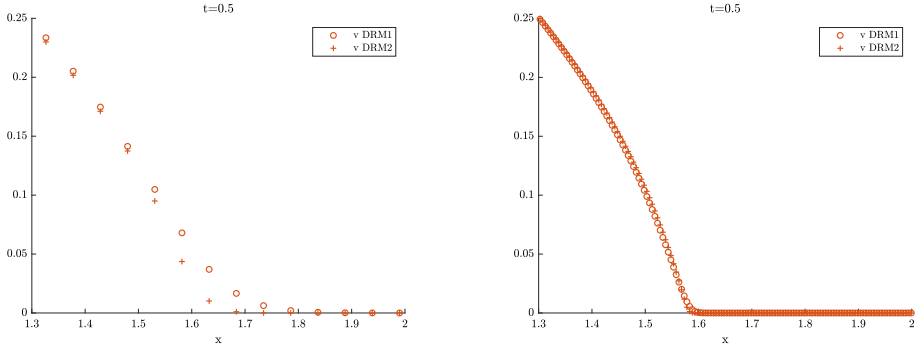

Fig. 13 Comparison between the DRM1 (circles) and the DRM2 (crosses) model close to the shock for the Buckley Leverett equation (103) for $\Delta x = 0.05$ (on the left) and $\Delta x = 0.0125$ (on the right)

4.8 A Three-Phase Flow Model with Gravitational Effect

We consider again the advection-diffusion Buckley-Leverett equation of the same form

$$\partial_t u + \partial_x f(u) = \xi \partial_{xx} B(u), \tag{107}$$

where now the flux function is given by

$$f(u) = \frac{u^2}{u^2 + a\,(1-u)^2}(1 - g\,(1-u)^2), \tag{108}$$

where a is the ratio of the viscosities of the two fluids and g is the gravitational effect. In this test the parabolic term has the form

$$B(u) = \begin{cases} 0, & \text{if } u < 0, \\ \xi\left(2u^2 - \frac{4}{3}u^3\right) & \text{if } 0 \le u \le 1, \\ \frac{2}{3}\xi & \text{if } u > 1. \end{cases} \tag{109}$$

Following [30], we set the following initial condition

$$u_0(x) = \begin{cases} 0, & \text{if } 0 \le x \le 1 - \frac{1}{\sqrt{2}}, \\ 1, & \text{if } \frac{1}{\sqrt{2}} < x \le 1. \end{cases} \tag{110}$$

We propose some numerical simulations for different values of g. We set the scaling factor $\xi = 0.01$ and the relaxation parameter $\varepsilon = 10^{-7}$. The spatial numerical grid is chosen $\Delta x = 0.01$ in $[0, 1]$ and the projective integration parameters are $\delta t = \varepsilon$, $K = 2$ and Δt chosen according to the CFL condition (64). In Fig. 14 and Fig. 15 we observe the results for $g = 0$ and $g = 5$ respectively at time $t = 0.05$ and $t = 0.1$.

4.9 A Two-Dimensional Three-Phase Model

As last example, we consider the two-dimensional Buckley-Leverett equation with diffusion, of the form

$$\partial_t u + \partial_x f_1(u) + \partial_y f_2(u) = \xi\left(\partial^2_{xx} u + \partial^2_{yy} u\right), \tag{111}$$

where the scaling factor $\xi = 0.01$ and the flux functions are

$$f_1(u) = \frac{u^2}{u^2 + (1-u)^2}, \qquad f_2(u) = f_1(u)\left(1 - 5(1-u)^2\right). \tag{112}$$

The initial condition is given by

$$u(x, y, 0) = \begin{cases} 1, & \text{if } x^2 + y^2 < 0.5, \\ 0 & \text{otherwise.} \end{cases} \tag{113}$$

The domain is $[-1.5, 1.5] \times [-1.5, 1.5]$ and the spatial discretization is obtained taking $\Delta x = \Delta y = 0.015$. The parameters for the projective integration method are the same as before, namely $\delta t = \varepsilon$, $\Delta t = C\Delta x^2$ and $K = 2$, where $C = 0.4$. Since this simulation has a discontinuous initial condition in two dimensions which may lead to oscillatory behavior, we employ a CWENO3 approximation for the hyperbolic variables, following the scheme [36].

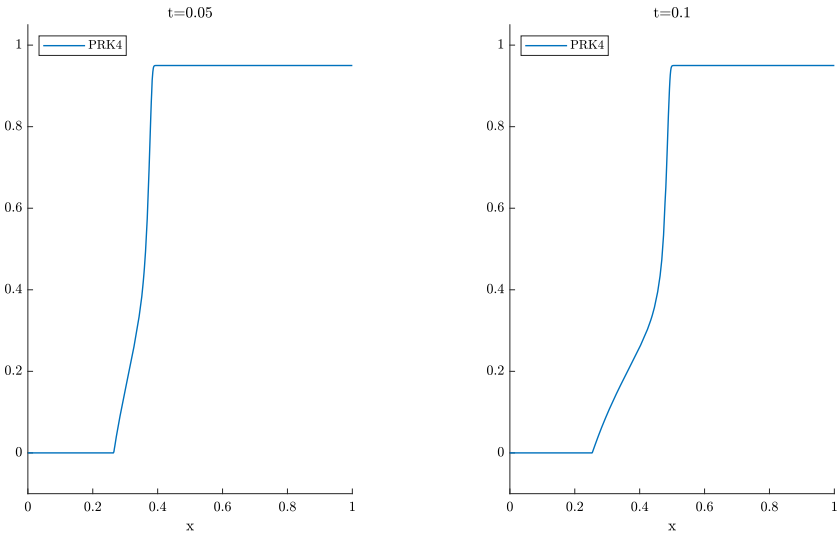

Fig. 14 Numerical approximation of the Buckley-Leverett with diffusion (109) with $g = 0$ at two different times $t = 0.05$ and $t = 0.1$

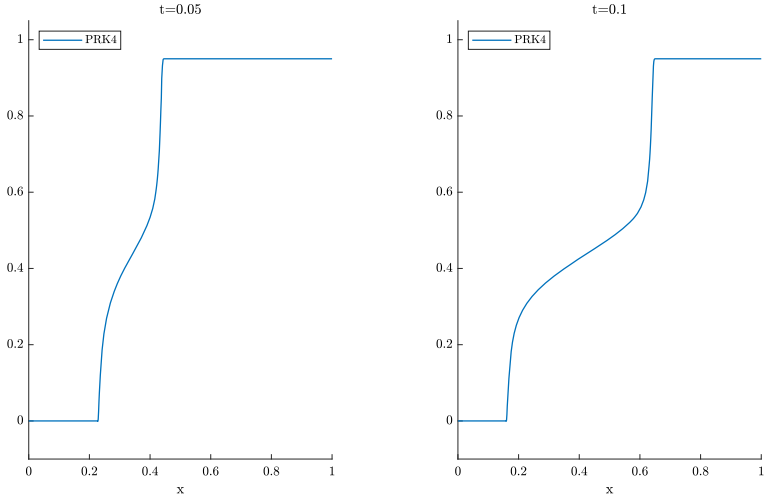

Fig. 15 Numerical approximation of the Buckley-Leverett with diffusion (109) with $g = 5$ at two different times $t = 0.05$ and $t = 0.1$

The results at time $t = 0.5$ agree with the ones of [31]. We underline again that the advantage of using relaxation schemes relies on their easily extensibility to the multi-dimensional case, without increasing the complexity of the numerical scheme. (See Figure 16).

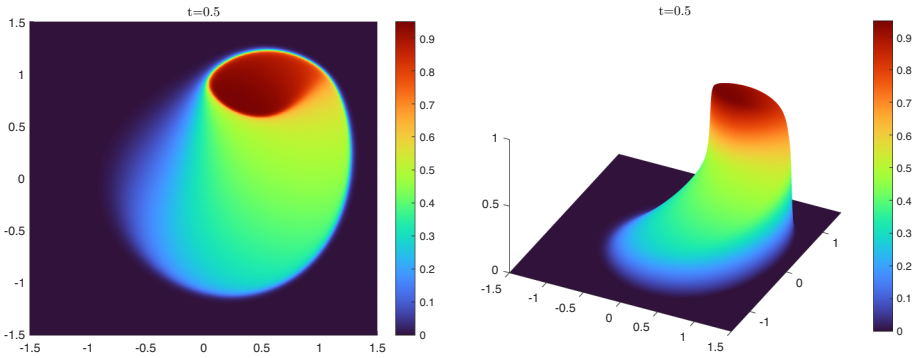

Fig. 16 Numerical approximation of the Buckley-Leverett with diffusion (111) at final time $t = 0.5$ with $\Delta x = \Delta y = 0.015$

5 Conclusion

In this paper, we have proposed an explicit arbitrary high-order scheme for the solution of discrete kinetic approximations of advection-diffusion equations. Indeed, the stiffness due to the presence of a relaxation operator could be treated with a projective integration approach, in order to avoid implicit time integration. We have analysed the spectrum of the discrete BGK approximation, to identify stable parameters for the projective integration scheme. Several numerical simulations in one and two spatial dimensions have been proposed, and the order of accuracy has been validated along with the computation of the speed up, compared to other methods.

The idea of using projective integration methods for discrete kinetic approximation could be easily extended to other types of equations (e.g. incompressible Navier-Stokes equation [14, 15] or moment models [27, 28]). Indeed, relaxation schemes have a deep connection with lattice Boltzmann Methods (LBM), see for instance [4, 5, 23, 53]. In a very recent paper, the theory of discrete kinetic BGK approximation of hyperbolic problems has been used to prove monotonicity properties for the LBM with overrelaxation [4]. This approach could be extended to the case of possibly degenerate parabolic equations and the computational performance of LBM could be compared (or coupled) with the projective integration approach.

Appendix A Runge-Kutta Methods

In Section 3 we have presented a higher order extension of projective integration schemes based on Runge-Kutta (RK) methods. Let us recall the main properties of RK methods. We consider an explicit S-stage RK method for a general equation of the form

$$y' = f(t, y), \qquad y(t_0) = y_0. \tag{114}$$

Let us consider a time step discretization given by Δt, then we have

$$\begin{cases} f^{n+c_s} = f^n + \Delta t \sum_{l=1}^{s-1} a_{s,l} \mathbf{k}_l, \\ \mathbf{k}_s = f\left(t^n + c_s\, \Delta t,\, f^{n+c_s}\right), \end{cases} \qquad 1 \le s \le S. \tag{115}$$

The matrix $\mathbf{A} = (a_{s,l})_{s,l=1}^{S}$ is the so-called *Runge-Kutta matrix*, the vector $\mathbf{b} = (b_s)_{s=1}^{S}$ and $\mathbf{c} = (c_s)_{s=1}^{S}$ are the *Runge-Kutta weights* and the *Runge-Kutta nodes*, respectively. The weights $\mathbf{b}_s$ and $\mathbf{c}_s$ are chosen to ensure consistency of the method, requiring $0 \leq b_s \leq 1$ and $0 \leq c_s \leq 1$ and

$$\sum_{s=1}^{S} b_s = 1, \sum_{s=1}^{S-1} a_{s,l} = c_s, \quad 1 \leq s \leq S. \tag{116}$$

Here we represent the Bucther's tableaux used in this paper, where we first recall the general form:

$$\begin{array}{c|c} c & A \\ \hline & b^T \end{array}$$

Now, we give detailed expressions of the Runge-Kutta tableaux for the third and the fourth order methods.

– Third-order SSP Runge-Kutta

$$\begin{array}{c|ccc} 0 & & & \\ 1 & 1 & & \\ 1/2 & 1/4 & 1/4 & \\ \hline & 1/6 & 1/6 & 2/3 \end{array}$$

– Classical fourth-order Runge-Kutta method

$$\begin{array}{c|cccc} 0 & & & & \\ 1/2 & 1/2 & & & \\ 1/2 & 0 & 1/2 & & \\ 1 & 0 & 0 & 1 & \\ \hline & 1/6 & 1/3 & 1/3 & 1/6 \end{array}$$

Appendix B Stability of the Inner Integrators

In this section we prove the result on the spectrum of the inner integrator, partially retracing the proof in [32]. The main difference are the non-constant ε-dependent coefficient in front of the entries D_j and the values of the Maxwellians M_j.

Theorem 1 *The spectrum of the matrix $\mathcal{A}$ defined in Section 3.1 satisfies*

$$Sp(\mathcal{A}) \subset \mathcal{D}\left(0, C\sqrt{\varepsilon}(|\xi| + |\gamma|)\right) \cup \{\zeta(\varepsilon)\}, \tag{117}$$

where C is a constant depending on the entries of D, ξ and γ are defined in (51) and $\zeta(\varepsilon)$ is the dominant eigenvalue.

Proof In the first step we use Rouché's Theorem to localize the eigenvalues, whereas in the second step we give the explicit asymptotic expansion for the dominant eigenvalue. We have obtained the following expression for the characteristic polynomial of $\mathcal{A}$,

$$\chi_{\mathcal{A}}(\zeta) = \prod_{i=1}^{4}(-\varepsilon D_i - \zeta)\left(1 - \frac{1}{4}\sum_{j=1}^{4}\frac{M_j}{\zeta - \varepsilon D_j}\right). \tag{118}$$

The expression for the characteristic polynomial of matrix $\mathcal{A}_0 := D + P$ is given instead by

$$\chi_{\mathcal{A}_0}(\zeta) = \prod_{i=1}^{4}(-\varepsilon D_i - \zeta)\left(1 - \frac{1}{4}\sum_{j=1}^{4}\frac{1}{\zeta - \varepsilon D_j}\right). \tag{119}$$

The idea is to study the behavior of the rational function

$$\mathcal{F} : \zeta \to \frac{\chi_{\mathcal{A}(\zeta)} - \chi_{\mathcal{A}_0}(\zeta)}{\chi_{\mathcal{A}_0}(\zeta)} = -\frac{\frac{1}{4}\sum_{j=1}^{4}(M_j - 1)\frac{1}{\zeta - \varepsilon D_j}}{1 - \frac{1}{4}\sum_{j=1}^{4}\frac{1}{\zeta - \varepsilon D_j}} \tag{120}$$

and to observe the regions containing eigenvalues of $\mathcal{A}_0$ for which $|\mathcal{F}(\zeta)| < 1$.

Here, we just point out some aspects of the computation which differ from the original one.

- Let us first consider the dominant eigenvalue of $\mathcal{A}_0$, restricting the analysis to the region parametrized by $\Omega_1 := \left\{1 + \varepsilon\, r\, e^{i\theta}, \theta \in [0, 2\pi)\right\}$, performing a Taylor expansion of $\dfrac{1}{1 + \varepsilon\, r\, e^{i\theta} - \varepsilon\, D_j}$ in terms of ε:

$$\frac{1}{1 + \varepsilon\, r\, e^{i\theta} - \varepsilon\, D_j} = 1 + \left(\varepsilon\, D_j - \varepsilon\, r\, e^{i\theta}\right) + \mathcal{O}(\varepsilon^2).$$

  We observe that

$$\sum_{j=1}^{4}(M_j - 1) = 0. \tag{121}$$

  The rational function $\mathcal{F}$ could be expanded as

$$\mathcal{F}(1 + \varepsilon\, r\, e^{i\,\theta}) = -\frac{\frac{1}{4}\sum_{j=1}^{4}(M_j - 1)\, D_j + \mathcal{O}(\varepsilon)}{r\, e^{i\,\theta} - \frac{1}{4}\sum_{j=1}^{4} D_j + \mathcal{O}(\varepsilon)}. \tag{122}$$

  Thus, choosing $r > \dfrac{1}{4}\left|\sum_j D_j\right| + \dfrac{1}{2}\left|\sum_j D_j\,(M_j - 1)\right|$, we ensure that $|\mathcal{F}(\zeta)| < 1/2 + \mathcal{O}(\varepsilon)$. From Rouché's Theorem, in Ω_1 (around $\zeta = 1$), $\chi_{\mathcal{A}}$ and $\chi_{\mathcal{A}_0}$ have the same number of zeroes, which means that $\mathcal{A}$ have only one eigenvalue in Ω_1.
- We focus now on the remaining eigenvalues, by considering the region around $\zeta = 0$, which contains the "fast" eigenvalues of $\mathcal{A}_0$. Then, we restrict the analysis to the region $\Omega_2 := \left\{\varepsilon r\, e^{i\,\theta},\ \theta \in [0, 2\pi)\right\}$ and we perform a Taylor expansion of $\dfrac{1}{r\, e^{i\,\theta} - D_j}$ in terms of $1/r$:

$$\frac{1}{r\, e^{i\,\theta} - D_j} = \frac{e^{-i\theta}}{r} + \frac{D_j\, e^{-i\,2\theta}}{r^2} + \mathcal{O}\left(\frac{1}{r^3}\right).$$

Using again (121), the rational function $\mathcal{F}$ could be now expanded as

$$\mathcal{F}(\varepsilon\, r\, e^{i\,\theta}) = -\frac{\frac{1}{4}\sum_{j=1}^{4}(M_j - 1)\, D_j \dfrac{e^{-i\,2\,\theta}}{r^2} + \mathcal{O}\left(\dfrac{1}{r^3}\right)}{4\varepsilon - \dfrac{e^{-i\,\theta}}{r} + \mathcal{O}\left(\dfrac{1}{r^2}\right)}$$
$$= -\frac{e^{-i\,\theta}}{r}\frac{\frac{1}{4}\sum_{j=1}^{4}(M_j - 1)\, D_j + \mathcal{O}\left(\dfrac{1}{r}\right)}{4\varepsilon\, r\, e^{i\,\theta} - 1 + \mathcal{O}\left(\dfrac{1}{r}\right)}.$$

We finally perform a Taylor expansion in terms of ε, to obtain

$$\mathcal{F}(\varepsilon\, r\, e^{i\,\theta}) = \frac{e^{-i\,\theta}}{r}\frac{1}{4}\sum_{j=1}^{4}(M_j - 1)\, D_j + \mathcal{O}(\varepsilon). \tag{123}$$

Again, choosing $r > \dfrac{1}{2}\left|\sum_j D_j\right| + 1$, we ensure the inequality $|\mathcal{F}(\zeta)| < 1/2$ and we conclude using Rouché's Theorem that in Ω_2 (around $\zeta = 0$), $\chi_{\mathcal{A}}$ and $\chi_{\mathcal{A}_0}$ have the same number of zeroes, which means that $\mathcal{A}$ have $J - 1$ eigenvalues in Ω_2.

In the second step we give an asymptotic expression for the largest eigenvalue in terms of ε. We start from the expression of $\chi_{\mathcal{A}}$ given in (118). If $\zeta(\varepsilon)$ is a root of $\chi_{\mathcal{A}}$, it holds

$$\tilde{\chi}_{\mathcal{A}}(\zeta) := 1 - \frac{1}{4}\sum_{j=1}^{4}\frac{M_j}{\zeta - \varepsilon\, D_j} = 0. \tag{124}$$

Let us consider an expression of ζ in terms of its real coordinates, namely

$$\zeta(\varepsilon) = x(\varepsilon) + i\, y(\varepsilon) \tag{125}$$

and let us consider the asymptotic expansion of $x(\varepsilon)$ an $y(\varepsilon)$ in terms of ε:

$$x(\varepsilon) = x_0 + \varepsilon\, x_1 + \varepsilon^2\, x_2 + \mathcal{O}(\varepsilon^3), \qquad y(\varepsilon) = y_0 + \varepsilon\, y_1 + \varepsilon^2\, y_2 + \mathcal{O}(\varepsilon^3).$$

We plug these expansions in (124) and we perform a Taylor series expansion in terms of ε. Since $\zeta(\varepsilon)$ is a root for $\tilde{\chi}_{\mathcal{A}}$, all the coefficients of equal power in ε must vanish. For the zeroth order term we have

$$1 - \frac{1}{4}\sum_{j=1}^{4}\frac{M_j}{x_0 + i\, y_0} = 0, \tag{126}$$

which, since $\sum_j (M_j - 1) = 0$ implies

$$\frac{x_0}{x_0^2 + y_0^2} = 1 \qquad -\frac{y_0}{x_0^2 + y_0^2} = 0,$$

namely $x_0 = 1$ and $y_0 = 0$. Let us now determine the terms of order ε, using

$$\frac{1}{4}\sum_{j=1}^{4} M_j\left[(x_1 + i\, y_1) + D_j\right] = 0,$$

which implies

$$x_1 = \left(1 - \frac{1}{\theta^2}\right)\alpha + \frac{1}{\theta^2\sqrt{\varepsilon}}\xi, \qquad y_1 = \frac{1}{\lambda}\beta.$$

Finally, let us consider the second order terms in ε^2

$$\frac{1}{4}\sum_{j=1}^{4} M_j \left[(x_1 + i\, y_1)^2 + 2\, D_j^2 + 4(x_1 + i\, y_1)\, D_j - 2(x_2 + i\, y_2)\right] = 0,$$

for which we obtain

$$x_2 = 2(x_1^2 - y_1^2) + 2\left(1 - \frac{1}{\theta^2}\right)(\alpha^2 - \beta^2) + \frac{2}{\varepsilon\theta^2}(\xi^2 - \gamma^2),$$

$$y_2 = 4x_1\, y_1 + 2\frac{1}{\lambda}\alpha\,\beta.$$

□

Appendix C Stability of Higher Order Projective Integration

Let us recall here the stability properties of the projective Runge-Kutta methods. In order to compute the linear stability regions, the Dahlquist equation is introduced

$$\dot{y} = \lambda\, y, \qquad \mathrm{Re}(\lambda) < 0, \tag{127}$$

whose general solution does not blow up in time. Introducing a general inner integrator for this equation

$$y^{k+1} = \tau(\lambda\delta t) y^k, \tag{128}$$

we call $\tau(\lambda\delta t)$ the *amplification factor* of the inner integrator. Applying explicit time integration to equation (127), we observe that

$$y^{k+1} = \tau^{k+1}\, y_0, \tag{129}$$

which means that the inner integrator is linearly stable if $|\tau| \leq 1$. In the case of forward Euler integrator, we have $\tau(\lambda\delta t) = 1 + \lambda\,\delta t$. The goal of this section is to determine the values of τ for which the projective integration method is also stable. Let us first focus on projective Forward-Euler method applied to (127), which can be written as

$$y^{n+1} = \sigma(\tau, \Delta t, \delta t, K)\, y^n, \tag{130}$$

where the amplification factor σ is given by

$$\sigma^{\mathrm{PFE}}(\tau, \Delta t, \delta t, K) = \left[\left(\frac{\Delta t - (K+1)\,\delta t}{\delta t} + 1\right)\tau - \frac{\Delta t - (K+1)\delta t}{\delta t}\right]\tau^k. \tag{131}$$

The PFE method is stable if $|\sigma^{\mathrm{PFE}}(\tau, \Delta t, \delta t, K)| \leq 1$. The main goal of introducing a projective integration approach is to use a time step $\Delta t = \mathcal{O}(\Delta x^{\gamma})$. In the limit $\varepsilon \to 0$ for fixed Δx, we look at the limiting stability regions as $\Delta t/\delta t \to \infty$. In [20] it has been shown that the values τ satisfying (131) lie in the union of two separated disks $\mathcal{D}_1^{\mathrm{PFE}} \cup \mathcal{D}_2^{\mathrm{PFE}}$, where

$$\mathcal{D}_1^{\mathrm{PFE}} = \mathcal{D}\left(1 - \frac{\delta t}{\Delta t}, \frac{\delta t}{\Delta t}\right), \qquad \mathcal{D}_2^{\mathrm{PFE}}\left(0, \left(\frac{\delta t}{\Delta t}\right)^{\frac{1}{K}}\right), \tag{132}$$

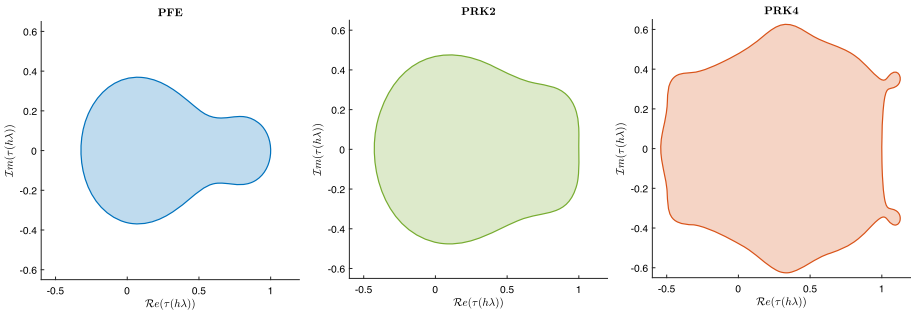

Fig. 17 Stability region for higher order projective integrators in the complex $h\lambda$-plane for $\Delta t/\delta t = 10$

and $\mathcal{D}(c, r)$ denotes the ball with center $(c, 0)$ and radius r in the complex λ-plane.

For higher order projective Runge-Kutta (PRK) schemes, it is possible to give an explicit expression of the *amplification factor*, applying the integrator to Equation (127). For the sake of simplicity, we introduce

$$M = \frac{\Delta t - (K+1)\delta t}{\delta t}, \quad \text{and} \quad M_s = \frac{c_s\,\Delta t - (K+1)\delta t}{\delta t}, \tag{133}$$

where c_s are the RK nodes. We also denote by $\mathbf{A} = (a_{s,l})_{s=1}^{S}$ and $\mathbf{b} = (b_s)_{s=1}^{S}$ the RK matrix and the RK weights for a general S-stage Runge-Kutta method. Then, for an explicit PRK method, we have

$$\begin{cases} \mathbf{k}_1 = \kappa_1(\tau) y^n = \dfrac{\tau^{K+1} - \tau^K}{\delta t}\, y^n, \\ \mathbf{k}_s = \kappa_s(\tau) y^n = \dfrac{\tau^{K+1} - \tau^K}{\delta t} \left(\tau^{K+1} + (M_s\,\delta t) \displaystyle\sum_{l=1}^{s-1} \frac{a_{s,l}}{c_s} \kappa_l \right) y^n, \qquad 2 \le s \le S, \\ y^{n+1} = \sigma(\tau)\, y^n = \left(\tau^{K+1} + (M\,\delta t) \displaystyle\sum_{s=1}^{S} b_s\, \kappa_s \right) y^n. \end{cases} \tag{134}$$

The following result on the stability of higher order projective Runge-Kutta methods holds.

Theorem 3 ([32], Theorem 3.2) *Assume the inner integrator is stable, i.e.* $|\tau| \le 1$ *and* δt, Δt *and* K *are chosen such that the projective forward Euler method is stable. Then, a projective Runge-Kutta method is also stable if it satisfies the following assumption*

$$\sum_{s=1}^{S} b_s = 1, \sum_{s=1}^{S-1} a_{s,l} = c_s, \quad 1 \le s \le S, \tag{135}$$

with $0 \le b_s,\ c_s \le 1$ *and the convexity condition*

$$0 \le a_{s,l} \le c_s, \qquad \forall\, 1 \le l \le s, \quad \forall\, 1 \le s \le S. \tag{136}$$

In Fig. 17-18 we show the stability regions of projective Runge-Kutta schemes for different values of $\delta t/\Delta t$ and K. The main feature, as proven in Theorem 3, is that the qualitative dependence of higher order PRK methods on the parameters is equivalent to those of PFE.

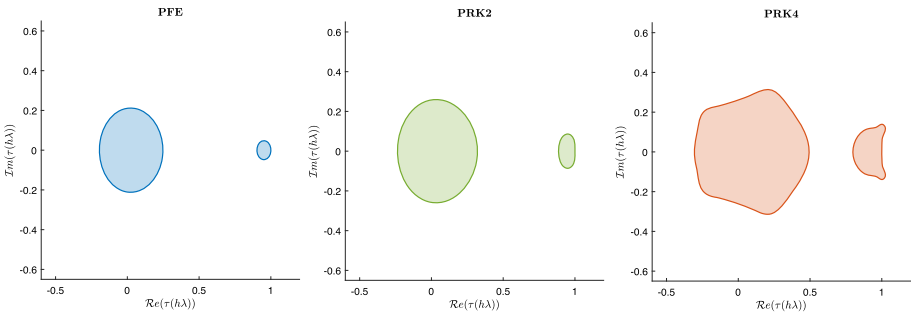

Fig. 18 Stability region for higher order projective integrators in the complex $h\lambda$-plane for $\Delta t/\delta t = 25$

Acknowledgements The author would like to thank Thomas Rey and Giuseppe Visconti for comments on this manuscript and for their careful reading. He would also like to thank Roberto Natalini and Giovanni Samaey for fruitful discussions on this topic. Finally, the author would like to thank the anonymous Reviewers for their careful reading and for their comments, which improved the quality of this work. The author is funded by the European Union's Horizon Europe research and innovation programme under the Marie Skłodowska-Curie Doctoral Network DataHyking (Grant No.101072546) and he is member of GNCS-INdAM research group.

Funding Open access funding provided by Università degli Studi di Roma La Sapienza within the CRUI-CARE Agreement.

Data Availability Data sharing not applicable to this article as no datasets were generated or analysed during the current study.

Declarations

Conflict of interest The author declares that he has no financial or non-financial conflicts of interest that are relevant to the content of this article.

References

1. Abgrall, R., De Santis, D., Ricchiuto, M.: High-order preserving residual distribution schemes for advection-diffusion scalar problems on arbitrary grids. SIAM J. Sci. Comput. **36**(3), a955–a983 (2014)
2. Amrita, A., Koellermeier, J.: Projective integration for hyperbolic shallow water moment equations. Axioms **11**, 5 (2022)
3. Arbogast, T., Wheeler, M.F., Zhang, N.-Y.: A nonlinear mixed finite element method for a degenerate parabolic equation arising in flow in porous media. SIAM J. Numer. Anal. **33**(4), 1669–1687 (1996)
4. Aregba-Driollet, D.: Convergence of lattice Boltzmann methods with overrelaxation for a nonlinear conservation law. ESAIM, Math. Model. Numer. Anal. **58**(5), 1935–1958 (2024)
5. Aregba-Driollet, D., Bellotti, T.: Monotonicity and convergence of two-relaxation-times lattice Boltzmann schemes for a non-linear conservation law. SIAM J. Numer. Anal. **64**(1), 251–276 (2026)

6. Aregba-Driollet, D., Natalini, R.: Discrete kinetic schemes for multidimensional systems of conservation laws. SIAM J. Numer. Anal. **37**(6), 1973–2004 (2000)
7. Aregba-Driollet, D., Natalini, R., Tang, S.: Explicit diffusive kinetic schemes for nonlinear degenerate parabolic systems. Math. Comput. **73**(245), 63–94 (2004)
8. Bailo, R., Rey, T.: Projective and telescopic projective integration for non-linear kinetic mixtures. J. Comput. Phys. **458**, 24 (2022)
9. Benton, E.R., Platzman, G.W.: A table of solutions of the one-dimensional Burgers equation. Q. Appl. Math. **30**, 195–212 (1972)
10. Bessemoulin-Chatard, M., Filbet, F.: A finite volume scheme for nonlinear degenerate parabolic equations. SIAM J. Sci. Comput. **34**(5), b559–b583 (2012)
11. Boscarino, S., Pareschi, L., Russo, G.: Implicit-explicit methods for evolutionary partial differential equations (to appear), vol. 24 of Math. Model. Comput. Philadelphia, PA: Society for Industrial and Applied Mathematics (SIAM) (2024)
12. Bouchut, F.: Construction of BGK models with a family of kinetic entropies for a given system of conservation laws. J. Stat. Phys. **95**(1–2), 113–170 (1999)
13. Bouchut, F., Guarguaglini, F.R., Natalini, R.: Diffusive BGK approximations for nonlinear multidimensional parabolic equations. Indiana Univ. Math. J. **49**(2), 723–749 (2000)
14. Bouchut, F., Jobic, Y., Natalini, R., Occelli, R., Pavan, V.: Second-order entropy satisfying BGK-FVS schemes for incompressible Navier-Stokes equations. SMAI J. Comput. Math. **4**, 1–56 (2018)
15. Carfora, M.F., Natalini, R.: A discrete kinetic approximation for the incompressible Navier-Stokes equations. ESAIM, Math. Model. Numer. Anal. **42**(1), 93–112 (2008)
16. Cavalli, F., Naldi, G., Puppo, G., Semplice, M.: High-order relaxation schemes for nonlinear degenerate diffusion problems. SIAM J. Numer. Anal. **45**(5), 2098–2119 (2007)
17. Cercignani, C.: The Boltzmann equation and its applications, vol. 67 of Appl. Math. Sci. New York etc.: Springer-Verlag (1988)
18. Diaz, J.I., Kersner, R.: On a nonlinear degenerate parabolic equation in infiltration or evaporation through a porous medium. J. Differ. Equations **69**, 368–403 (1987)
19. Ferretti, R.: A fully semi-Lagrangian technique for viscous and dispersive conservation laws. J. Comput. Phys. **526**, 113784 (2025)
20. Gear, C.W., Kevrekidis, I.G.: Projective methods for stiff differential equations: problems with gaps in their eigenvalue spectrum. SIAM J. Sci. Comput. **24**(4), 1091–1106 (2003)
21. Gear, C.W., Kevrekidis, I.G.: Telescopic projective methods for parabolic differential equations. J. Comput. Phys. **187**(1), 95–109 (2003)
22. Golub, G., Van Loan, C.F.: Matrix computations., 3rd edn., vol. 43 of Texts Read. Math. New Delhi: Hindustan Book Agency (2007)
23. Graille, B.: Approximation of mono-dimensional hyperbolic systems: a lattice Boltzmann scheme as a relaxation method. J. Comput. Phys. **266**, 74–88 (2014)
24. Jin, S., Pareschi, L., Toscani, G.: Diffusive relaxation schemes for multiscale discrete-velocity kinetic equations. SIAM J. Numer. Anal. **35**(6), 2405–2439 (1998)
25. Jin, S., Xin, Z.: The relaxation schemes for systems of conservation laws in arbitrary space dimensions. Commun. Pure Appl. Math. **48**(3), 235–276 (1995)
26. Karlsen, K.H., Lie, K.-A., Natvig, J.R., Nordhaug, H.F., Dahle, H.K.: Operator splitting methods for systems of convection-diffusion equations: nonlinear error mechanisms and correction strategies. J. Comput. Phys. **173**(2), 636–663 (2001)
27. Koellermeier, J., Samaey, G.: Projective integration schemes for hyperbolic moment equations. Kinet. Relat. Models **14**(2), 353–387 (2021)
28. Koellermeier, J., Samaey, G.: Spatially adaptive projective integration schemes for stiff hyperbolic balance laws with spectral gaps. SMAI J. Comput. Math. **8**, 295–325 (2022)
29. Koellermeier, J., Samaey, G.: Projective integration methods in the Runge-Kutta framework and the extension to adaptivity in time. J. Comput. Appl. Math. **454**, 26 (2025)
30. Kossaczká, T., Ehrhardt, M., Günther, M.: A neural network enhanced weighted essentially non-oscillatory method for nonlinear degenerate parabolic equations. Phys. Fluids **34**(2), 026604 (2022)
31. Kurganov, A., Tadmor, E.: New high-resolution central schemes for nonlinear conservation laws and convection-diffusion equations. J. Comput. Phys. **160**(1), 241–282 (2000)
32. Lafitte, P., Lejon, A., Samaey, G.: A high-order asymptotic-preserving scheme for kinetic equations using projective integration. SIAM J. Numer. Anal. **54**(1), 1–33 (2016)
33. Lafitte, P., Melis, W., Samaey, G.: A high-order relaxation method with projective integration for solving nonlinear systems of hyperbolic conservation laws. J. Comput. Phys. **340**, 1–25 (2017)
34. Lafitte, P., Samaey, G.: Asymptotic-preserving projective integration schemes for kinetic equations in the diffusion limit. SIAM J. Sci. Comput. **34**(2), a579–a602 (2012)

35. Lattanzio, C., Natalini, R.: Convergence of diffusive BGK approximations for nonlinear strongly parabolic systems. Proc. R. Soc. Edinb., Sect. A, Math. **132**(2), 341–358 (2002)
36. Levy, D., Puppo, G., Russo, G.: A third order central WENO scheme for 2d conservation laws. Appl. Numer. Math. **33**(1–4), 415–421 (2000)
37. Lions, P.L., Perthame, B., Tadmor, E.: A kinetic formulation of multidimensional scalar conservation laws and related equations. J. Am. Math. Soc. **7**(1), 169–191 (1994)
38. Lions, P.L., Toscani, G.: Diffusive limit for finite velocity Boltzmann kinetic models. Rev. Mat. Iberoam. **13**(3), 473–513 (1997)
39. Liu, Y., Shu, C.-W., Zhang, M.: High order finite difference WENO schemes for nonlinear degenerate parabolic equations. SIAM J. Sci. Comput. **33**(2), 939–965 (2011)
40. Melis, W., Rey, T., Samaey, G.: Projective and telescopic projective integration for the nonlinear BGK and Boltzmann equations. SMAI J. Comput. Math. **5**, 53–88 (2019)
41. Melis, W., Samaey, G.: Telescopic projective integration for linear kinetic equations with multiple relaxation times. J. Sci. Comput. **76**(2), 697–726 (2018)
42. Naldi, G., Pareschi, L.: Numerical schemes for kinetic equations in diffusive regimes. Appl. Math. Lett. **11**(2), 29–35 (1998)
43. Naldi, G., Pareschi, L.: Numerical schemes for hyperbolic systems of conservation laws with stiff diffusive relaxation. SIAM J. Numer. Anal. **37**(4), 1246–1270 (2000)
44. Naldi, G., Pareschi, L., Toscani, G.: Relaxation schemes for partial differential equations and applications to degenerate diffusion problems. Surv. Math. Ind. **10**(4), 315–343 (2002)
45. Natalini, R.: Convergence to equilibrium for the relaxation approximations of conservation laws. Commun. Pure Appl. Math. **49**(8), 795–823 (1996)
46. Natalini, R.: A discrete kinetic approximation of entropy solutions to multidimensional scalar conservation laws. J. Differ. Equations **148**(2), 292–317 (1998)
47. Natalini, R., Ribot, M., Twarogowska, M.: A numerical comparison between degenerate parabolic and quasilinear hyperbolic models of cell movements under chemotaxis. J. Sci. Comput. **63**(3), 654–677 (2015)
48. Pareschi, L., Russo, G.: Implicit-explicit Runge-Kutta schemes and applications to hyperbolic systems with relaxation. J. Sci. Comput. **25**(1–2), 129–155 (2005)
49. Pomraning, G.C., Foglesong, G.M.: Transport-diffusion interfaces in radiative transfer. J. Comput. Phys. **32**, 420–436 (1979)
50. Richardson, L.F.: IX. The approximate arithmetical solution by finite differences of physical problems involving differential equations, with an application to the stresses in a masonry dam. Philos. Trans. R. Soc. Lond. Ser. A, Contain. Papers Math. Phys. Character **210**(459–470), 307–357 (1911)
51. Shu, C.-W.: Essentially non-oscillatory and weighted essentially non-oscillatory schemes for hyperbolic conservation laws. In: Advanced numerical approximation of nonlinear hyperbolic equations. Lectures given at the 2nd session of the Centro Internazionale Matematico Estivo (C. I. M. E.) held in Cetraro, Italy, June 23–28, 1997. Berlin: Springer, pp. 325–432 (1998)
52. Wissocq, G., Abgrall, R.: A new local and explicit kinetic method for linear and non-linear convection-diffusion problems with finite kinetic speeds. I: One-dimensional case. J. Comput. Phys. **518**, 29 (2024)
53. Wissocq, G., Liu, Y., Abgrall, R.: A positive- and bound-preserving vectorial lattice Boltzmann method in two dimensions. SIAM J. Sci. Comput. **47**(6), A3276–A3302 (2025)
54. Zhang, Q., Wu, Z.-L.: Numerical simulation for porous medium equation by local discontinuous Galerkin finite element method. J. Sci. Comput. **38**(2), 127–148 (2009)